Comparison of silver-plated nylon (Ag/PA66) e-textile and Ag/AgCl electrodes for bioelectrical impedance analysis (BIA)

Irini Logothetis[1], Ignacio Gil[2], Xungai Wang[1] and Joselito Razal[1]

[1] Institute of Frontier Materials, Deakin University, Geelong, Australia
[2] Department of Electronic Engineering, Universitat Politecnica de Catalunya, Terrassa (Barcelona), Spain

E-mail: rena.logothetis@deakin.edu.au

Received xxxxxx
Accepted for publication xxxxxx
Published xxxxxx

Abstract

Recently, researchers have adapted Bioelectrical Impedance Analysis (BIA) as a new approach to objectively monitor wounds. They have indicated various BIA parameters associated to specific wound types can be linked to wound healing through trend analysis relative to time. However, these studies are conducted using wet electrodes which have been identified as possessing several shortcomings, such as unstable measurements. Thus, the adaption of e-textile electrodes has become an area of interest in measuring biosignals. E-textile electrodes are known to possess a significantly large polarization impedance (Z_p) that potentially influences these biosignal measurements. In this study we aim to identify the suitability of e-textile electrodes to monitor wounds using BIA methodologies. By adapting suggested methodologies conducted in-vivo from previous studies, we used an ex-vivo model to observe the behaviour of e-textile electrodes relative to time. This was compared to common clinical wet electrodes, specifically Ag/AgCl. The objective of this study was to identify the BIA parameters that can be used to monitor wounds with e-textile electrodes. By analysing the BIA parameters relative to time, we observed the influence of Z_p on these parameters.

Keywords: electronic textile electrodes (e-textile electrodes), dry electrodes, Bioelectrical impedance analysis (BIA), polarization impedance, biopotential electrodes, wearable electrodes

1. Introduction

Current clinical wound management is poorly managed and is of major concern [1–4]. Practitioners and nurses monitor the wound healing process in accordance with the Australian and New Zealand standards for wound prevention and management [5]. However, this methodology cannot be quantified. It is based on visual assessment that can potentially lead to a misdiagnosis resulting in improper treatment of the wound [6–10]. The current protocol of managing wounds can also be timely requiring the aid of multiple measuring tools [11]. These shortcomings have resulted in infections and ulcers due to premature withdrawal of treatments. It is an issue that has impacted government expenditure, in addition to the patient's 'out-of-pocket' cost and quality of life. A vast amount of research has been undertaken into monitoring wounds using Bioelectrical Impedance Analysis (BIA) adapting wet electrodes as the interface between the system and the skin. With the development of microtechnology and

conductive threads, the concept of wearable technology [12–14] adapting smart textile sensors for long-term monitoring of wounds is a possibility.

Currently, research into BIA for wounds adapt wet electrodes such as Ag/AgCl. These electrodes are manufactured with a 'gel' electrode-electrolyte layer that prevents a charge build up from the injected current through a redox-reaction; thus, they are regarded as nonpolarized [15]. However, previous research has indicated that these electrodes are subjected to a minor polarization [16,17] that is considered negligible. Therefore, wet electrodes can be adapted to all biomedical systems regardless of its frequency range (0.5 Hz to 1 MHz) [18]. This is evident in research adapting ECG electrodes for BIA measurements. These electrodes possess an adhesive layer securing them to the skin. However, to create a secure interface between the electrodes and the skin thorough preparation of the skin is required. In addition, this adhesive layer can irritate the skin. Moreover, the 'gel' and adhesive layer are subject to dehydration relative to time. This could potentially be due to a degradation of the 'gel' layer altering the redox reaction and the loss of adhesiveness altering the interface pressure between the electrode and skin. Inconsistent dehydration of paired electrodes causes an electrode mismatch resulting in unstable and unreliable measurements. Research suggests that an electrode-mismatch could influence the symmetry of the Cole plot associated with multi-frequency BIA (mfBIA) by presenting a 'hook' artefact for the frequency range of 3-1000 kHz [19,20].

To overcome these shortcoming of wet electrodes, dry electrodes have recently received much attention. Dry electrodes have been developed with the use of polymers and nanoparticles in the form of membranes [21–36] and textiles [37–53]. However, recently research has suggested that polymers can cause skin irritations while nanoparticles can enter the body through the skin's pores. Embroidering electronic textile (e-textile) electrodes is a simple and convenient fabrication process resulting in comfortable dry electrodes without the shortcomings of the previously mentioned dry electrodes. However, an issue pertaining to e-textile electrodes is by passing a current through the electrodes, a charge build-up occurs on the surface causing a polarization impedance (Z_p). This is a common phenomenon across all dry electrodes; thus, they are classified as polarized electrodes [18,54–58]. The Z_p associated with e-textile electrodes is significantly greater than wet electrodes, specifically by a magnitude of kΩ. Moreover, the Z_p is frequency dependent indicating that the fabrication and performance of e-textile electrodes is system dependent.

Our previous research on e-textile electrodes demonstrated the impact of the fabrication process and substrate selection on Z_p for single frequency BIA (sfBIA) at a discrete frequency of 50 kHz. Adapting a wafer experimental methodology, we measured the autonomous Z_p of electrode pairs. Our study into the fabrication process indicated an increase in the surface area of the e-textile electrodes resulted in a reduction in Z_p. Moreover, we were able to further reduce Z_p by increasing the stitch length and stitch density (reduction in stitch spacing). This study was followed by analysing a suitable substrate based on the impact of changes in skin properties relative to Z_p. A climatic chamber was adapted to imitate the skin properties, specifically skin temperature and perspiration. We observed that the Z_p of the e-textile electrodes with a polyester non-woven substrate was the least impacted relative to changes in skin temperature and perspiration.

The Z_p can potentially influence measurements of the biotissue under study (BUS) due to an unstable electrode-skin impedance (Z_{es}). A comparison of Z_{es} between wet and dry electrodes was studied by Spach et al. for a frequency range between 6 Hz and 1 kHz [59]. This study demonstrated a significantly lower Z_{es} associated with wet electrodes compared to dry electrodes [59]. This could be associated with the low frequency ranges associated with ECG measurements. It has been suggested that these frequency ranges are susceptible to unwanted noise [60]. A vast amount of research into monitoring wounds using BIA adapt frequencies above 1 kHz [61–63].

1.1 BIA parameters

BIA systems measure the electrical resistance of the BUS through its response to an external electric current [64–69]. It is simple and non-invasive method that observes trends relative to the wound healing process [70,71] by applying a discrete frequency, referred to as single frequency BIA (sfBIA) or a frequency sweep known as multi-frequency BIA (mfBIA). sfBIA measures the impedance modulus ($|Z|$), resistance (R), reactance (X_C), phase angle (φ) at the selected frequency. mfBIA finds the characteristic frequency (f_C) where the body's reactance is at its maximum and uses this frequency to determine the paremeters in addition to the short and open circuit resistance (R_0 and R_{inf}, respectively) [72–75]. R_0 and R_{inf} relate to the extra cellular fluid resistance and intracellular fluid resistance of the BUS modelled in parallel at a frequency of 0 for R_0 and at infnite frequency for R_{inf}. At these two frequency extremes, the cell membrane causes the capacitance of the BUS to behave as an open and short circuit. The impedance modulus is referred to as Z throughout this paper. The equations associated with Z and φ are defined by Equation 1 and Equation 3:

$$Z = \sqrt{R^2 + X_C^2}, \quad \text{Equation 1}$$

where

$$X_C = \frac{1}{2\pi f C}. \quad \text{Equation 2}$$

$$\varphi = tan^{-1}\frac{X_C}{R}, \quad \text{Equation 3}$$

where f is the frequency (interchangeable with f_C for mfBIA) and C is the capacitance of the BUS at that frequency.

The overall capacitance consists of the setup of the metallic textile electrodes and the BUS acting as a dielectric.

mfBIA is based on the Cole model represented by a resistance equivalent to the difference between R_0 and R_{inf} parallel to a constant phase element in series with R_{inf} [76] (Figure 1); where the constant phase element corresponds to the non-ideal capacitance of the cell membrane of the BUS. Plotting R and X_C on the x and y axis respectively across a frequency axis ranging from low to high f_C, Z, φ, R_0 and R_{inf} are extrapolated (Figure 2).

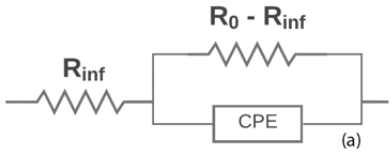

Figure 1. Cole model [77].

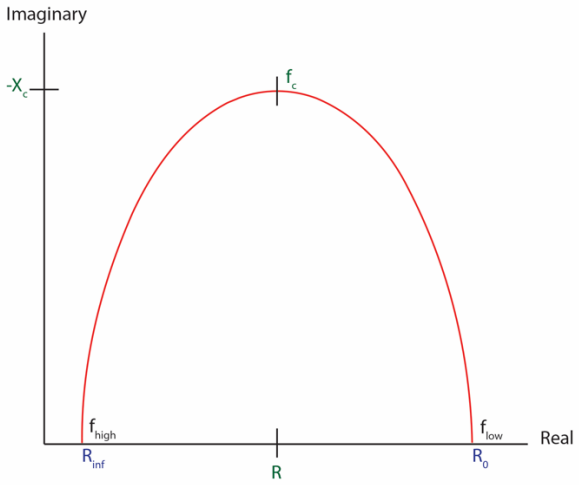

Figure 2. Cole plot [78].

1.2 Methods into monitoring wounds using BIA

Lukaski et al. adapted BIA to monitor the healing process of various wounds [62] focusing on trends relating to R, X_C and φ at a frequency of 50 kHz. The electrodes were positioned locally in a tetrapolar configuration adjacent to the wounds with 1 cm distance between the current injecting electrodes and associated voltage sensors. The intermediate distances between the inner voltage electrodes positioned on the edge of the wounds varied depending on the size of the wound. Lukaski et al. observed an increase in trends across all parameters for uncomplicated wounds as the wound healed. The surgical wound demonstrated a fluctuation in trend across all parameters relative to interventions. The infected wound indicated significant changes in the magnitude and direction of the parameter trends. This research suggested that R is indicative of successful wound healing while X_C and φ are related to neuropathy.

Muller et al.'s study on diabetic patients focused on lower limb ulcers [61]; however, the ulcer dimensions were not reported. ImpediMed's SFB7 was used with a frequency sweep ranging between 3-1000 kHz. A local tetrapolar electrode configuration was adapted with the voltage sensors positioned at the edge of the wound and the current injecting electrodes adjacently positioned with a distance of 1 cm. Adapting the Cole model, R and X_C were extracted for analysis. Muller et al. associates an increasing trend in Z relative to the wound healing process.

A frequency sweep and Cole model were also adapted on burn wounds by Kenworthy et al. using the same equipment [70,71,79] with a tetrapolar electrode configuration. These studies included: (i) a validation of the reliability of the equipment [70], (ii) performance based on the electrode positioning [70,79] and (iii) a correlation between BIA parameters and the healing phase [71]. R_0, R_{inf} and R_i were analysed for (i) – (ii), while for (iii) φ was added into the study. Kenworthy et al. concluded that the SFB7 was a reliable measuring instrument to monitor wounds regardless of the wound type. It was also suggested that local positioning of the electrodes performed best in comparison to whole body and segmental. The final study based on the BIA parameters, indicated that R_0 and R_{inf} are strongly related to the wound healing process contrary to R_i and φ. During the healing phase, an increasing trend in R_0 and R_{inf} is noticeable [71].

Kekonen et al. analysis discrete frequencies ranging from 10 Hz to 100 kHz [63]. Measurements were recorded once daily over numerous days depending on the wound. Initial studies were conducted in a bipolar configuration before transitioning to a tetrapolar configuration [80]. An electrode couple were placed on the wound and another couple on the surrounding undamaged skin [63,80,81] as reference points where the normalisation percentage ratio of the wound Z relative to undamaged skin Z was observed [82,83]. Kekonen et al. identified an increasing trend in Z relative to the wound healing [83].

King et al. studies inflammation of ankles due to acute ankle fractures [84] using sfBIA. This research was included in our study as inflammation is an important phase of the healing process [85]. The electrodes were positioned in a segmental tetrapolar configuration and Z was measured at 5 kHz and 200 kHz on the injured limb and the opposite uninjured limb. King et al. observed a significantly lower Z in the injured limb with relatively close measurements between 50 kHz and 200 kHz.

From this previous research, we identified the methodological adaption of BIA systems to monitor wounds. Local tetrapolar electrode configuration adjacent to the wound demonstrates an accurate method of measuring BIA parameters associated with the wound healing process. sfBIA

and mfBIA have been adapted with an emphasis on analysing the parameter trend relative to time for the BIA parameters [86] indicating the need to monitor a wound continuously. Adapting e-textile electrodes would assist for short-term and long-term monitoring.

In this study, we consider these methodologies adapted to monitor wounds using BIA in order to test the efficacy of e-textile electrodes compared to clinical electrodes. The first part of this paper identifies the shape of the e-textile electrodes that reduces Z_p. We then test the behaviour of pork belly in a bipolar and tetrapolar configuration relative to time using Ag/AgCl. Pork belly was selected as it emulates human skin due to its close dielectric properties. To evaluate the efficacy of the e-textile electrodes, we set up an experimental protocol based on the methodology from previous research to observe the trend of the BIA parameters used to monitor wounds relative to time. Comparing the e-textile electrodes to standard Ag/AgCl electrodes, we identified if the parameters were impacted by the high Z_p of e-textile electrodes.

2. Methodology

This research has three components where the first two sub-studies (i.e. Part A and Part B) are preliminary leading to the final section (Part C), refer to Figure 3. The first part is the fabrication and testing of elliptical and rectangular e-textile electrodes to identify the the shape that results in the lowest Z_p. The second part is a study into the behaviour of pork belly as a BUS to set up the time period for our final experiment. The final part studies the behaviour of measuring the BUS using the Ag/AgCl and e-textile electrodes with the BIA parameters suggested in previous research, specifically Z, R, R_0, R_{inf}, X_C and φ. These were measured for the discrete frequencies of 5 and 50 kHz and for a frequency sweep ranging from 3-1000 kHz with the Cole plot using the SFB7. The SFB7 measures R and X_C and calculates Z and φ, the system also applies a trademark algorithm to extrapolate R_0 and R_{inf}. All measurements were conducted in ambient room temperature, with a temperature of 20°C and a relative humidity of 60%.

2.1 Part A: E-Textile Electrodes

The e-textile electrodes were fabricated using the embroidery process reported in our previous studies. For the conductive component of the e-textile electrodes, Shieldex Conductive Yarn–Silver Plated Nylon (Ag/PA66) 2 × 117/17 dtex (Shieldex U.S., Palmyra, NY, United States) was used as the needle thread. This thread has a reported linear resistance of about 1500 $\Omega.m^{-1}$ and a linear density of 29.5 tex.

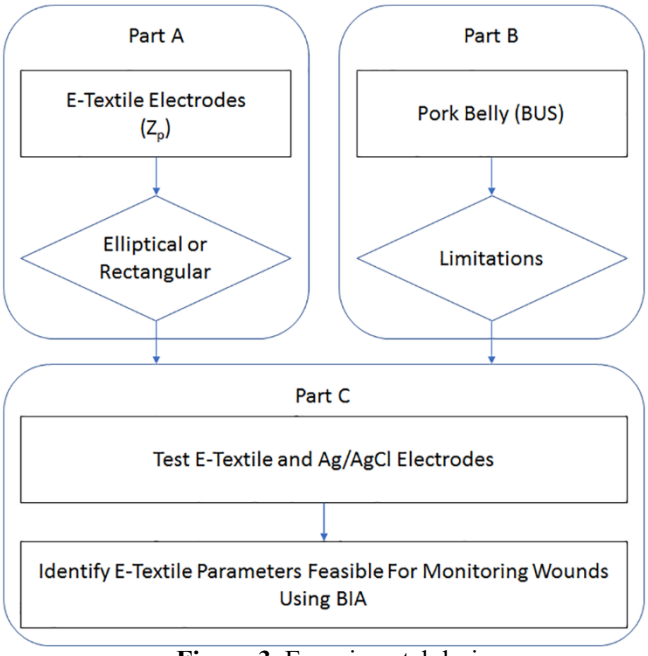

Figure 3. Experimental design.

Thus, we matched this thread to a 100% polyester (PES) thread with a linear density of 39.8 tex for the bobbin thread [58]. The electrodes were designed and fabricated using the Embrilliance Embroidery Digitizing Software and Brother F440E embroidery machine based on our previous findings [18,58,87]. Elleptical and rectangular electrodes were embroidered on a polyester non-woven felt (relative permittivity: ε_r = 1.2 [58]) with stitch length 7 mm, stitch spacing (density) 0.4 mm and a surface area of 13.2 cm^2. The dimensions and tolerances of electrodes were adjusted using embroidery process software, also snap-fasteners were attached to probes.

Twelve coupled electrodes were fabricated for each shape, labeled sets S-E1 to S-E12 for the elliptical and S-R1 to S-R12 for the rectangular e-textile electrodes. To test the Z_p of the e-textile electrodes, the triple-layer wafer method was adapted from our previous studies. For more information on the fabrication and testing methodologies, refer to our previous publications [18,58,87]. The e-textile electrodes were paired in a bipolar configuration with the conductive sides interfacing a polyester swatch of dimensions 45×40 mm and Z_p was measured with the PM 6306 LCR Meter (Fluke Australia Pty Ltd, New South Wales, Australia) at 50 kHz, a common frequency associated to BIA.

2.2 Part B and Part C: Preparation and Methodology

To test the electrodes pork belly was used as a BUS as its dielectric properties are comparable to human skin [88,89]. The samples were purchased from a local butcher fresh in the morning (the origin and purchase of the pork belly was in Melbourne, Australia). The BUS sample cross dimensional

measurements were about 20 × 18 × 4 cm and weighed about 1.5 kg. The samples were transported in a cooler without any ice to avoid cooling distribution that cannot be controlled. To repeat the experiment over two days, we refrigerated the pork belly. Each sample was wrapped in a natural calico textile and placed in air tight polyethylene storage sealable bags. The samples were placed adjacently on the grill shelves of the refrigerator and stored overnight at a temperature of 5°C.

The electrodes were commercially purchased. Ambu WhiteSensor WS Ag/AgCl electrodes were chosen due to their highly conductive solid gel, large surface area with strong adhesion and foam backing [90]. Given that Ag/AgCl electrodes requires preparation of the skin, we prepared the BUS samples by cleaning them using Isopropyl Alcohol swab wipes. The BUS samples were left to dry for an hour prior to placing the electrodes. A 10 minute period prior to taking measurements allowed the electrodes to settle and adhere to the skin [91]. We applied the frequency sweep of the SFB7 and set the device to collect 5 measurements every three seconds for each data collection. The absolute values for R, X_C, Z, φ and R_0 and R_{inf} were extracted directly from the BioImp software.

To analyse the Z relative to time, normalisation was applied to the BIA parameters with reference to the measured absolute value of the parameter under study at time 0 minutes, i.e. the first measurement, refer to Equation 4. It has been suggested that the rate of change of BIA parameters in relation to time are relatively small [92], therefore the normalisation was transformed to a percentage.

$$P_{ratio} = \frac{P_t}{P_0} \times 100\%, \qquad \text{Equation 4}$$

where P refers to the parameter of interest, P_t is the absolute value of the parameter at time t, while P_0 is the absolute value of the parameter at time 0. For example, analysing Z at 30 minutes, we would have the following:

$$Z_{ratio} = \frac{Z_{30}}{Z_0} \times 100\% \qquad \text{Equation 5}$$

To present this data, a 100% horizontal line is plotted referring to the absolute value at time 0 minutes (the time of the first data collected). Thus, at time 0 all parameters are located on the 100%, as time passes it indicates the deviation from this reference point. It is also important to note that a logarithmic scale could not be adapted for this study as the rate of change was relatively small. Although 3D density plots provide absolute values of the BUS Z and φ [93], normalisation was a preferred method of analysis to observe the trend (refer to section Methods into monitoring wounds using BIA).

2.2.1 Part B: Pork Belly Limitations. To gain a better understanding of the BUS, a preliminary experiment was performed to measure Z of the pork belly BUS in a tetrapolar and bipolar configuration with the electrodes positioned distally at 10 cm [75]. The bipolar configuration was used as a reference to test and compare our measured Z to previous research in the field of food and technology, refer to Appendix I. However, the focus of this study is based on a tetrapolar configuration common in BIA measurements of wounds. The Ag/AgCl electrodes were placed onto the pork belly, with the adhesiveness of the electrodes bounding the skin to the electrode.

For the preliminary experiment, measurements were collected every 30 minutes over a span of 180 minutes. We repeated this experiment over two days to observe the trend of the BUS sample that will be adapted for Part B. For the preliminary study, the data was analysed using the Cole plot with a frequency range of 3-1000 kHz and for the various pre-set discrete frequency measurements, specifically: 5, 50, 100 and 200 kHz. This analysis was completed for the common BIA parameters: Z, R, X_C and φ.

2.2.2 Part C: Testing of Ag/AgCl and Ag/PA66 e-textile electrodes. The primary focus of this study was to compare the performance of e-textile and Ag/AgCl electrodes for use with BIA systems to monitor wounds. To test the electrodes, six BUS samples were prepared. Three samples were measured using the wet electrodes and three with the dry elliptical electrodes over a two-day period. Table 1 lists the BUS samples dimensions of the BUS samples. The weight and measurements of the BUS samples and electrodes used. A 2 x 2 x 0.5 cm (length x width x depth) excision was created in the centre of the BUS sample as a guide for the positioning of the electrodes covered with a compression sleeve.

Table 1. Pork belly BUS samples for Part C.

BUS Sample	Weight (kg)	Dimensions: l × w × h (cm)	Electrodes
S1	1.5	20 × 17 × 4	Ag/AgCl
S2	1.5	20 × 17 × 4	Ag/AgCl
S3	1.5	20 × 17 × 4	Ag/AgCl
S4	1.5	20 × 18 × 4	S-E1, S-E2
S5	1.5	20 × 18 × 4	S-E3, S-E4
S6	1.5	20 × 17 × 4	S-E5, S-E6

The compression sleeve provided a relatively controlled methodology for the e-textile electrodes to conform to the BUS samples compared to other methods that were trialled on an independent sample. Various commercially available materials from haberdashery stores and chemists were tested. Given that the Ag/AgCl electrodes rely on the adhesiveness layer to bond to skin, we imitated this method with the e-textile electrodes by trying skin glue (also referred to liquid skin); however, the glue dehydrated and detached from the samples. Sports Strapping Tape, Micropore Paper Tape and

Surgical Tape did not provide strong adherence and the e-textile electrodes detached from the sample resulting in incorrect measurements due to motion artefact especially when attaching the leads to the electrodes. It is important to note that these methods were tested on pork belly; thus, it is possible that these methods may work on human skin. We tried Velcro, common in previous research on humans. However, the rigidness of Velcro did not allow the e-textile electrodes to conform to the shape and deep sulci of the pork belly sample creating an air gap between the electrode and the skin [57,94] resulting in erroneous measurements. This also occurred with a medium weight crepe bandage due to its large and incontrollable shear and stretch properties resulting in inconsistent pressures. The Elastocrepe Heavy Weight Crepe Bandage with a tighter textile structure reduced the sheerness and stretch providing more control. With a stretch of 60%, strips of the bandage were cut to half the width of the BUS samples and transformed into a compression sleeve by sewing the top and bottom edge of each strips together with a domestic sewing machine. However, in 'real-life' applications a more suitable approach would be to sew Velcro onto the edges of the bandage strips where the compression sleeve can be easily applied and removed without discomfort to the patient.

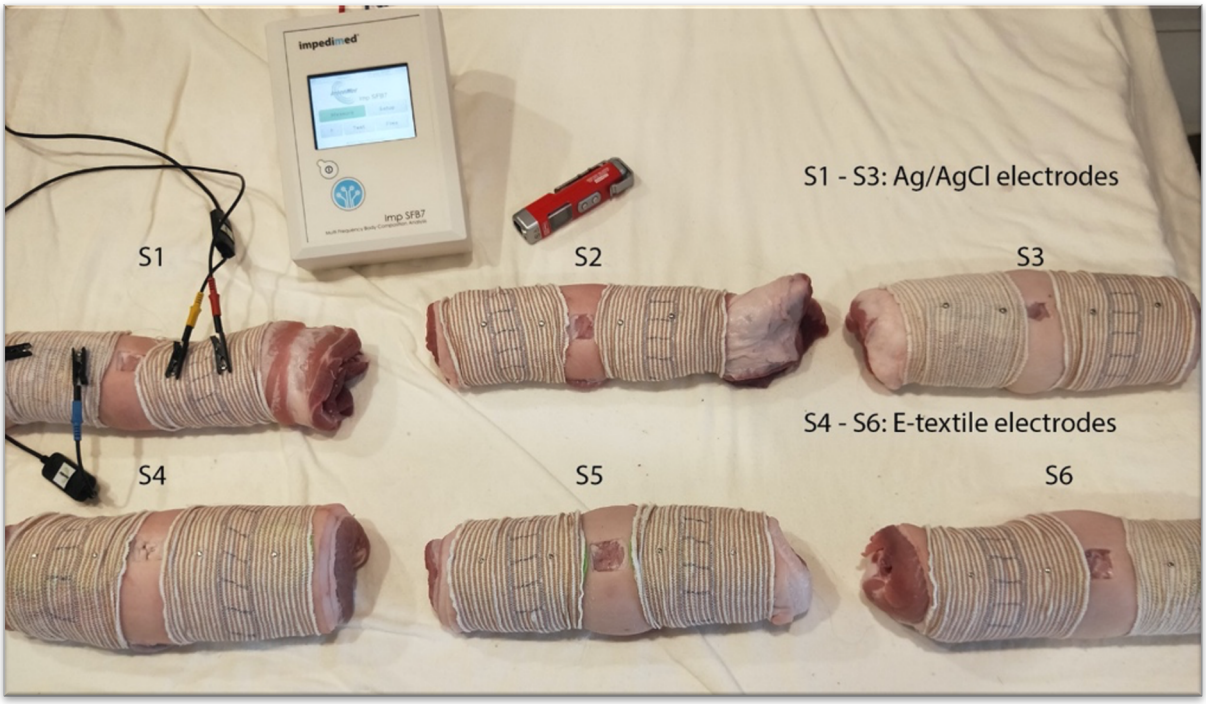

Figure 4. Experimental set-up for Part C.

Given that the Ag/AgCl electrodes adhere to the skin, there were no modifications required for the sleeves to be used with these electrodes. However, for the e-textile electrodes we carefully hand-sewed them to the sleeves. We avoided using the sewing machine to prevent the possibility of any damage to the conductive side from the sewing machine. By following the tetrapolar configuration, a set of e-textile electrodes acting as voltage sensors were sewn at the edge of the bandage while we positioned the other set of e-textile electrodes adjacent to the voltage sensors at a distance of 1 cm. These act as the current injecting electrodes. To create an ideal scenario we imitated the concave shape of a limb by rolling the BUS samples [95] (Figure 4) and passing it through the compression sleeve to maintain its shape. The sleeve was fitted with the voltage sensing electrodes positioned relatively close to the edge of the excision (i.e. about 0.5 cm).

For the BUS samples tested with Ag/AgCl electrodes, the unmodified sleeve was fitted first, maintaining the concave shape of the BUS sample prior to adhering the electrodes to the skin. The configuration for the Ag/AgCl was identical to the configuration of the e-textile electrodes. By placing the sleeve over the Ag/AgCl electrodes we attempted in applying a relatively consistent pressure across the Ag/AgCl electrodes and e-textile electrodes as this has an impact on their performance [94]. To facilitate for the connection of the SFB 7 leads, the snaps were passed through an opening of the sleeve.

The measuring methodology was based on Part B, and the time period was reduced to 60 minutes. Given that we reduced the experimental time, we also reduced the time period of the measurements to 15 minutes in order to obtain an adequate amount of data. A 15-minute time period also provides adequate time to collect and verify the data collected from the 6 samples. This experiment was also completed on two days as in Part B. After collecting the data at the end of day 1, we placed all the sleeves in the washing machine. To reduce the risk of causing any damage to the e-textile electrodes, the washing machine was set on delicate cycle with a cold water and 300 spin cycle setting. The sleeves were laid out to dry flat to avoid any stretch to the crepe bandage. Although the purpose of washing the sleeves was to test the efficacy of re-using the e-textile electrodes, we also washed the sleeves used with the Ag/AgCl electrodes. Given that it is possible for a slight change in the structure of the crepe textile bandage due to the washing process, it is important to maintain consistency across all sleeves for comparison of the two types of electrodes.

This experiment was customised based on the research currently undertaken in measuring wounds using BIA in terms of frequencies and BIA parameters analysed, refer to Figure 5.

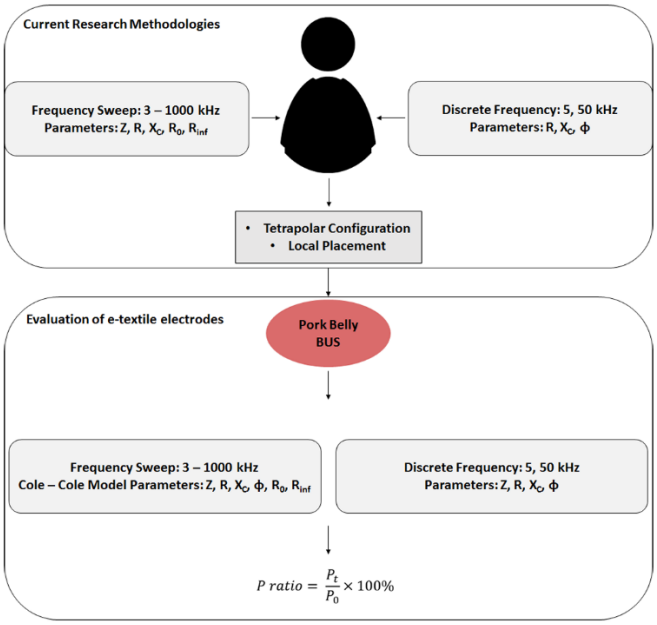

Figure 5. Experimental process.

3. Results

3.1 Part A: E-Textile Electrodes

By fabricating rectangular electrodes (S-R1 to S-R12) and the elliptical electrodes (S-E1 to S-E12) on the non-woven polyester substrates, we tested Z_p and φ. Measurements are presented in Figure 6. By testing the 12 sets for each shape, an average Z_p of 235.4 and 205.8 kΩ was observed for the rectangular and elliptical e-textile electrodes, respectively. The range between the sample sets was relatively low, close to 4% for both shapes. The elliptical electrodes possessed a Z_p 13.5% less than the rectangular electrodes (based on percentage difference not percentage change). This could be due to the elliptical shape having an even charge distribution across the surface area, while the charge on the rectangular e-textile electrodes potentially stray to the edges. φ of about -90º is indicative of a pure capacitive effect that is consistent across both shapes. Therefore, for Part C, we adapted the elliptical e-textile electrodes.

3.2 Part B: Pork Belly Limitations

The bipolar method has previously been adapted to measure Z of necrotic pork tissue [96] in the food and technology field measuring about 650 Ω at 50 kHz. This is comparable to our value of Z measuring 600 Ω at time 0 in the bipolar mode, refer to Appendix I for BUS properties and trend analysis. Therefore, this supports our method of measuring the pork BUS. Thus, we were able to conduct the experiments in a tetrapolar configuration common to BIA measurements on human beings. Z was measured to be about

70 Ω in a tetrapolar configuration. This is comparable to measurements on human beings in a tetrapolar configuration [72]; therefore, confirming the dielectric properties of pork belly skin.

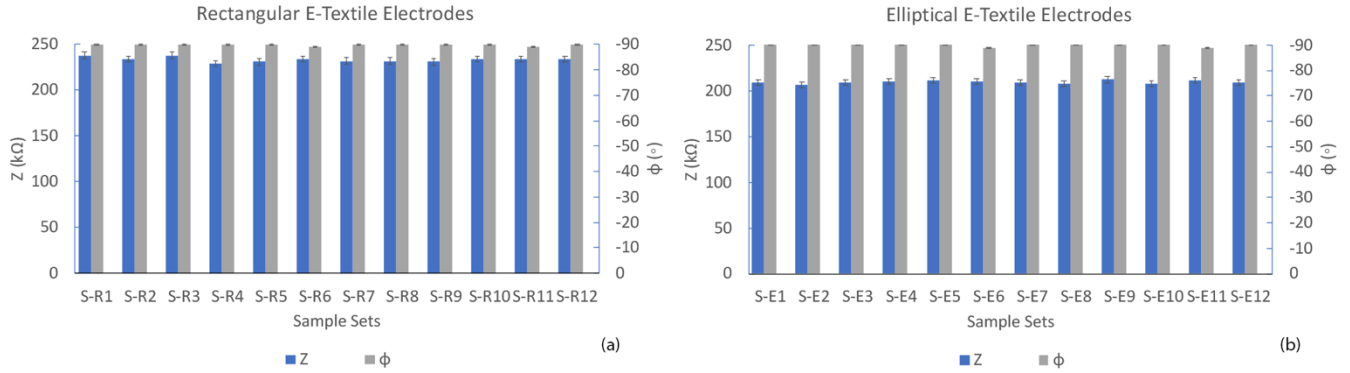

Figure 6. Measurements for e-textile electrodes: (a) Z_p and φ for rectangular electrodes and (b) Z_p and φ for elliptical electrodes.

In a tetrapolar configuration, Z and R demonstrated some saturation at 80% over a 180-minute period on the two days, refer to Figure 7a-b. This trend was identical for frequency sweep and the discrete frequencies. This decrease settles between 60 and 90 minutes. Although, an exponential decrease was not demonstrated for X_C and φ, and no trend was discernible, refer to Figures 7c-f. This could be caused by a parasitic capacitance [97]. This becomes prominent at higher frequencies, specifically 100 and 200 kHz.

Research suggests that an applied pressure to the electrodes can reduce the skin-electrode interface impedance [94,98,99]. However, this is outside the scope of this study and Part B was indicative of an exponential decrease occurring before settling. Research has indicated that there is a continuous change in Z relative to the wound healing; thus, we are interested in observing the period of change observed in the BUS of this study (i.e. the pork belly). Although the time before settling occurs between 60 and 90 minutes, we adapted 60 minutes for Part C. This was also a suggested time limit for keeping the BUS samples at room temperature suggested by experts in the food and technology industry.

3.3 Part C: Evaluation of Ag/AgCl and Ag/PA66 e-textile electrodes

3.3.1 Evaluation of e-textile electrodes for electrode mismatch. Despite a slight tolerance associated with the fabrication process, the Cole model was symmetrical for the frequency range 3-1000 kHz and no electrode-mismatch was observed, refer to Figure 8. This is indicative of the e-textile electrodes working with the SFB7. Therefore, a frequency range of 3-1000 kHz was able to be used for further analysis.

3.3.2 Evaluation of Z and R. Figure 9a-d present the trend for Z and R associated with the Ag/AgCl and e-textile electrodes over two days. Z and R were relatively identical for both electrode types across all the samples. For the Ag/AgCl electrodes a ratio difference at each measurement point was as low as 0.1% while for the e-textile electrodes, it was slightly greater with a difference between Z and R of about 0.4%. This variation between Z and R was negligible; thus, Z and R were presented on the same plot. The exponential decrease that was observed in Part A was also demonstrated in Part B. This exponential decrease over time has been associated to the electrode-skin impedance (Z_{es}) [100].

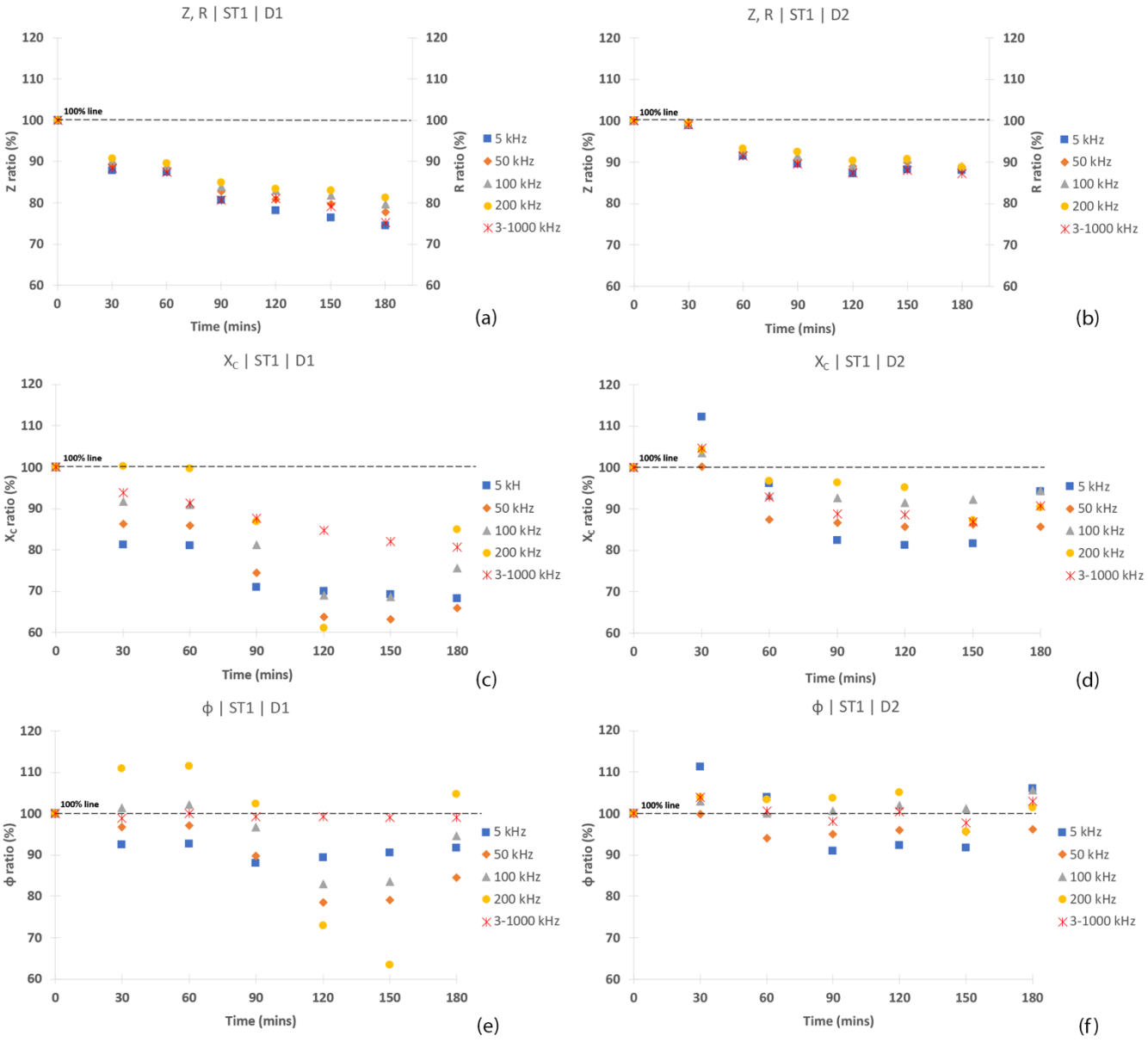

Figure 7. Measurements for intact BUS using Ag/AgCl in tetrapolar configuration: (a) *Z* and *R* day 1, (b) *Z* and *R* day 2 (c) X_C day 1, (d) X_C day, (e) φ day 1, (f) φ day 2.

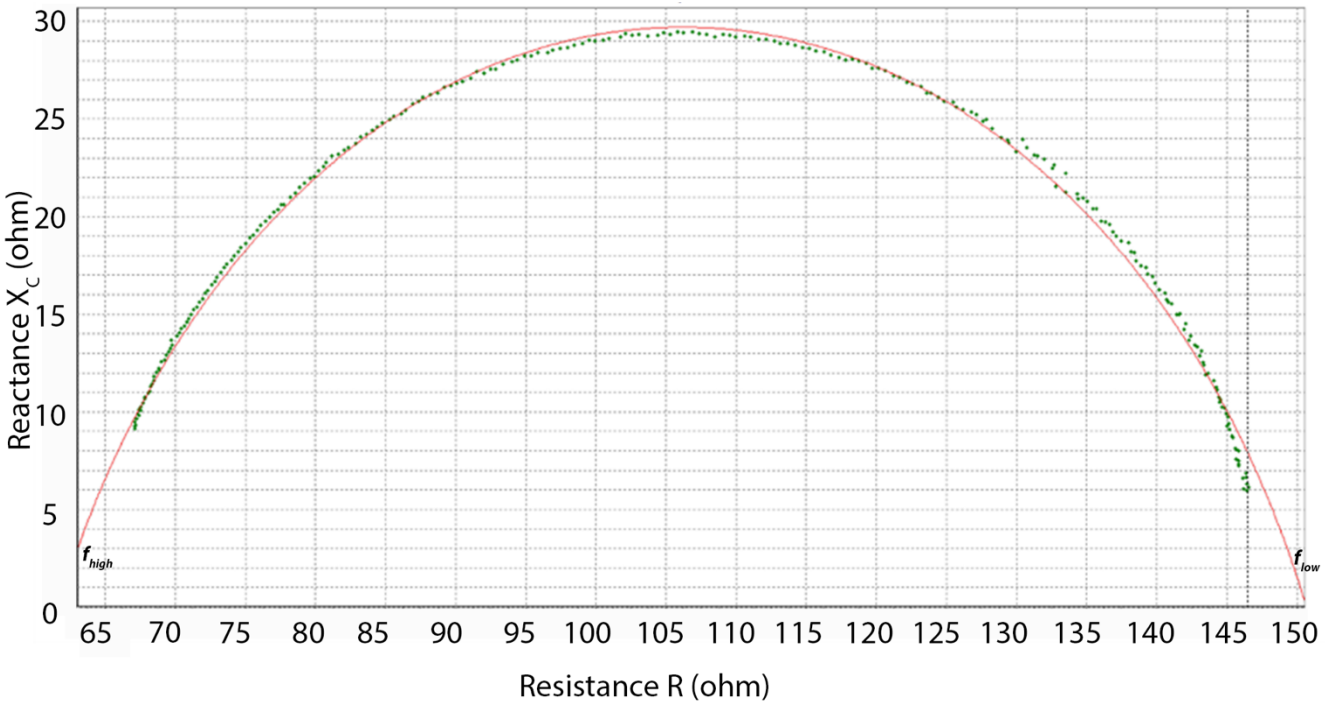

Figure 8. Cole plot for e-textile electrodes as presented by SFB7.

Regarding absolute values of *Z*, there is a difference across the samples; yet, the rate of change is identical. For the discrete frequency of 50 kHz commonly associated with BIA measurements [101], on day 1, time 0 the BUS samples S1, S2 and S3 resulted in *Z* of 152, 115 and 100 Ω respectively. For S4, S5 and S6, *Z* was 85, 115 and 110 Ω at 50 kHz, respectively. These values are with the compression sleeve and it is important to note that the pressure from the sleeves may cause a reduction in *Z* [102]. However, the compression sleeve was applied to all the samples in order to maintain consistency; the influence of pressure due to the compression sleeve is outside the scope of this study. This variance of *Z* across samples is also observed in human beings. It has been suggested that *Z* is dependent on the subject and is influenced by skin properties, such as skin thickness, skin moisture and hair in addition to the underlying soft biotissue (i.e. muscle and fat). For samples S1-S3 measured with Ag/AgCl electrodes, there is a 42% difference from the samples with the lowest and greatest *Z* values. This range is comparable to *Z* measurements in vivo from a wide range of subjects [74]. The *Z* of the samples measured with the e-textile electrodes showed a range of 25%. There is a possibility that the repeatability and quality measurement of the e-textile electrodes is higher than the conventional Ag/AgCl; however, this requires further analysis and is outside the scope of this paper. The variance in absolute values had no influence on the observed trend relative to time. These trends were identical across all samples for the frequency sweep, and discrete frequencies associated with Ag/AgCl and the e-textile electrodes, refer to Figures 9, 10 and 11 for the sweep and discrete frequencies 5 and 50 kHz respectively. Thus, this indicates that the performance of the e-textile electrodes is comparable to the Ag/AgCl. This is true regardless of whether a frequency sweep or the discrete frequencies of 5 and 50 kHz is adapted for analysis. Day 2 showed that by washing the e-textile electrodes, their performance was not compromised, refer to Figure 9c-d, 10c-d and 11c-d.

From this analysis, it is also clear that *R* is the principle factor of *Z* for both type of electrodes on necrotic tissue. Thus, it is safe to assume that the polarization impedance of the e-textile electrodes where X_C was the dominant factor had no influence on *Z*. A decrease of about 6-7% on day 1 and 16-17% on day 2 was observed over the 60-minute period across the samples for both types of electrodes. By applying exponential regression to the plots, the equations associated with the samples measured using the Ag/AgCl and e-textile electrodes were comparable with a strong correlation. Analysing the measurements over the two-day period and across the frequency sweep and discrete frequencies of 5 and 50 kHz, a strong correlation was observed. R^2 relating to S1-S3 ranged from 0.87-0.98 while for S4-S6 ranged from 0.82-0.99, refer to Table 1 in Appendix II.

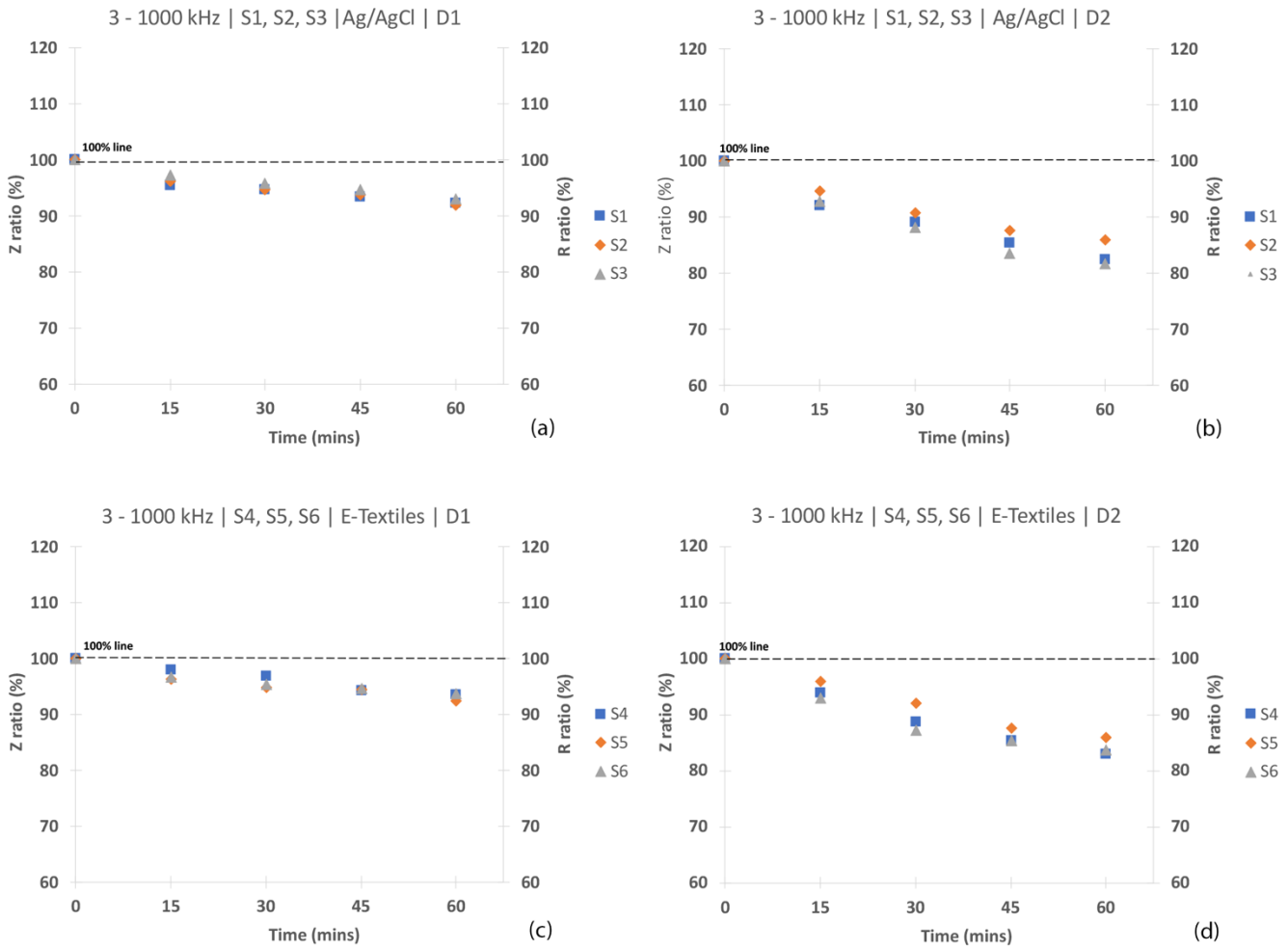

Figure 9. *Z* and *R* ratio relative to time at 3-1000 kHz sweep for electrodes: (a) Ag/AgCl day 1 and (b) day 2; (c) e-textiles day 1 and (d) day 2.

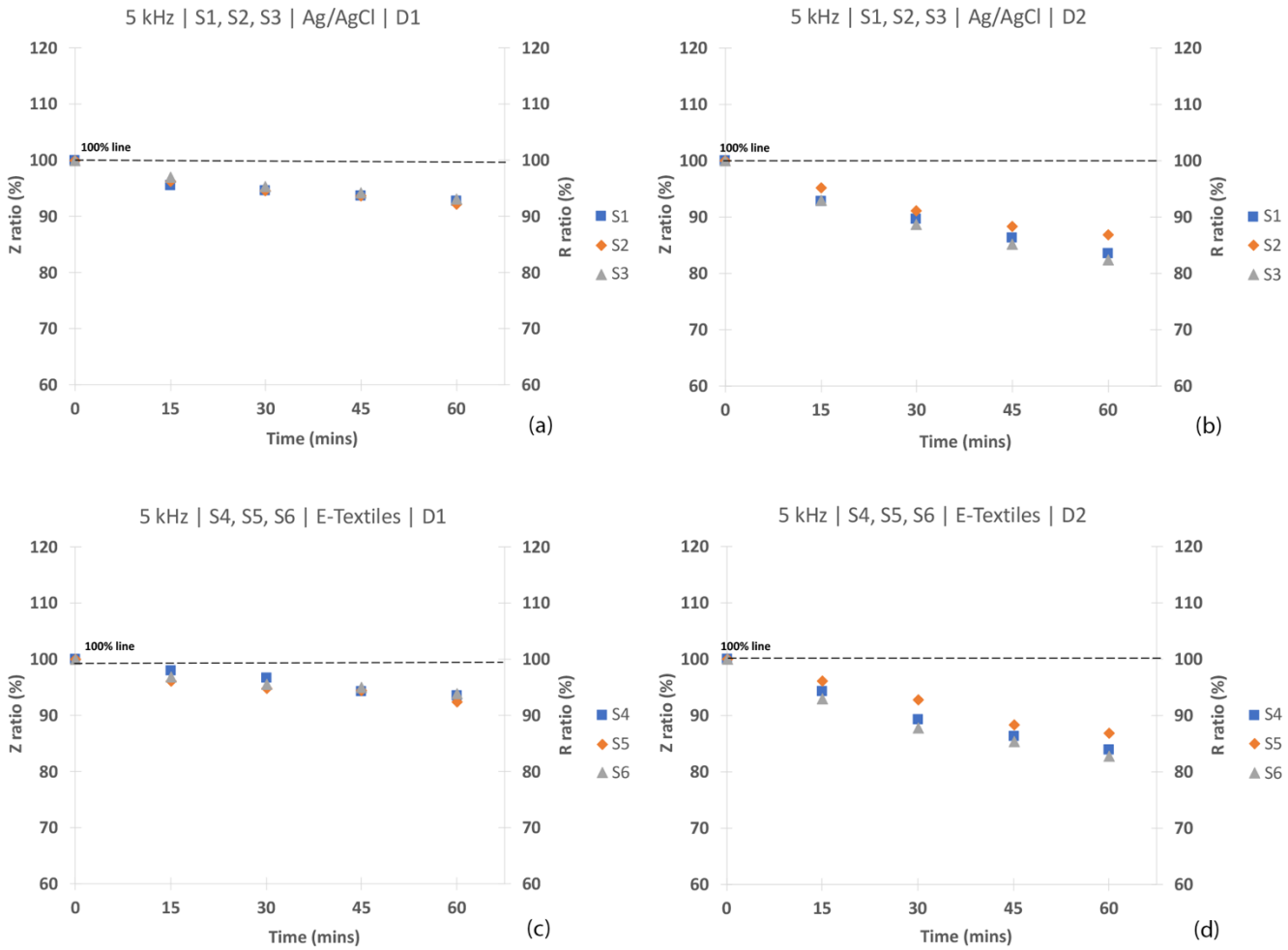

Figure 10. *Z* and *R* ratio relative to time at 5 kHz for electrodes: (a) Ag/AgCl day 1 and (b) day 2; (c) e-textiles day 1 and (d) day 2.

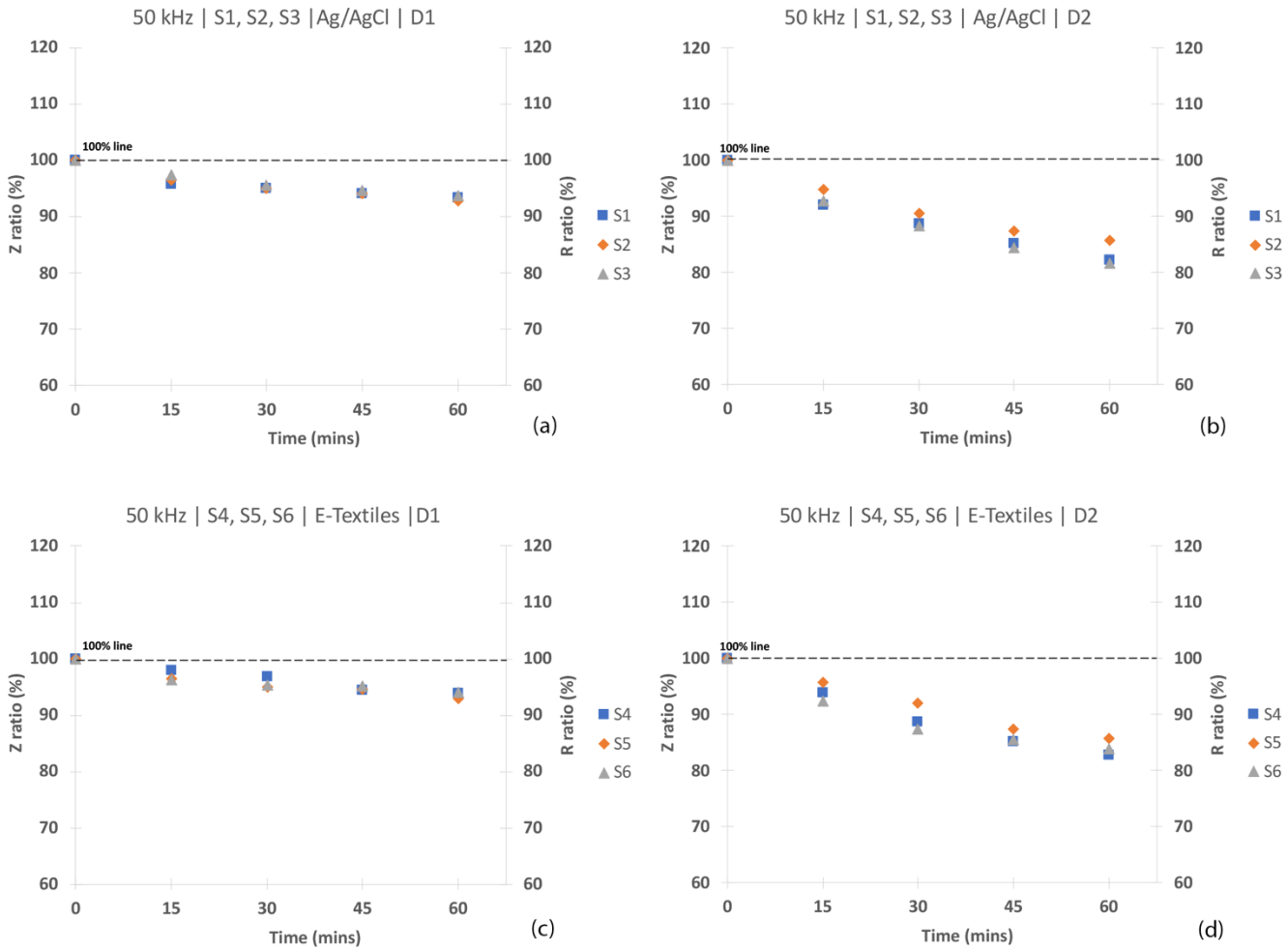

Figure 11. *Z* and *R* ratio relative to time at 50 kHz for electrodes: (a) Ag/AgCl day 1 and (b) day 2; (c) e-textiles day 1 and (d) day 2.

3.3.3 Evaluation of X_C. At 50 kHz (refer to Figure 14), on day 1 and at time 0 (i.e. initial measurement), the absolute values for X_C using the Ag/AgCl electrodes on S1, S2 and S3 were: 35, 30 and 25 Ω respectively; these values are equivalent to a capacitance of about 90, 105 and 125 nF. The X_C for samples S4, S5 and S6 using the e-textiles were: 9, 30 and 28 Ω respectively with equivalent capacitance values of 350, 105 and 115 nF.

Referring to Figure 12a, the frequency sweep analysed for the Ag/AgCl electrodes demonstrates a gradual exponential decrease on day 1 where $R^2 > 0.85$ (refer to Table 2, Appendix II). However, this is not demonstrated by samples S1 and S3 on day 2 where $R^2 = 0.33$, refer to Figure 12b and Table 2 Appendix II. For the discrete frequencies, 5 and 50 kHz there was no apparent exponential decrease on day 1, refer to Figure 13a and 14a. However, applying a regression, at 50 kHz there was a similarity in trend equations comparable to the frequency sweep where $R^2 > 0.72$. At 5 kHz, the trend equations were comparable to the frequency sweep and 50 kHz; however, for S1 and S2 R^2 was as low as 0.21 and 0.14 respectively. A decrease was observed on day 2 for 5 kHz across all samples (i.e. S1-S3) where $R^2 > 0.96$. At 50 kHz this was only observed for one sample S3 and $R^2 = 0.97$, refer to Figure 13b and 14b. However, a weak correlation was observed for S1 and S2 where $R^2 < 0.14$. Therefore, an inconsistency was observed for X_C associated with Ag/AgCl electrodes across the replicates on the two days.

The e-textile electrodes clearly do not display a trend, where a scattering of X_C is evident relative to time. This is demonstrated on all samples S4-S5 on both days. This scattering occurs with the frequency sweep and for the discrete frequencies 5 and 50 kHz, refer to figure 12c-d, 13c-d and 14c-d. However, S5 presented a moderate to strong correlation where $R^2 > 0.70$ across the two days for the various frequency settings. Thus, an inconsistency across the samples and frequency settings was also observed for the e-textile electrodes. Referring to Figure 8 in the Cole plot section, a

symmetrical Cole plot was observed for all measurements; thus, this scattering cannot be associated to a Z_{es} mismatch.

Despite the Ag/AgCl electrodes not demonstrating a consistent trend, X_C was significantly impacted for samples S4-S5 measured using the e-textile electrodes. This inconsistency with the Ag/AgCl and scattering associated with the e-textile electrodes could potentially be associated with unwanted noise. It is expected for this noise to have a greater impact on the e-textile electrodes given that the contact interface of the e-textile electrodes is highly conductive. This could also vary between samples due to the tolerance associated with the fabrication process of the e-textile electrodes [58]. It is also important to note that this scattering occurs on day 1 and day 2; hence, it is indicative of the e-textile electrodes not being affected by washing them.

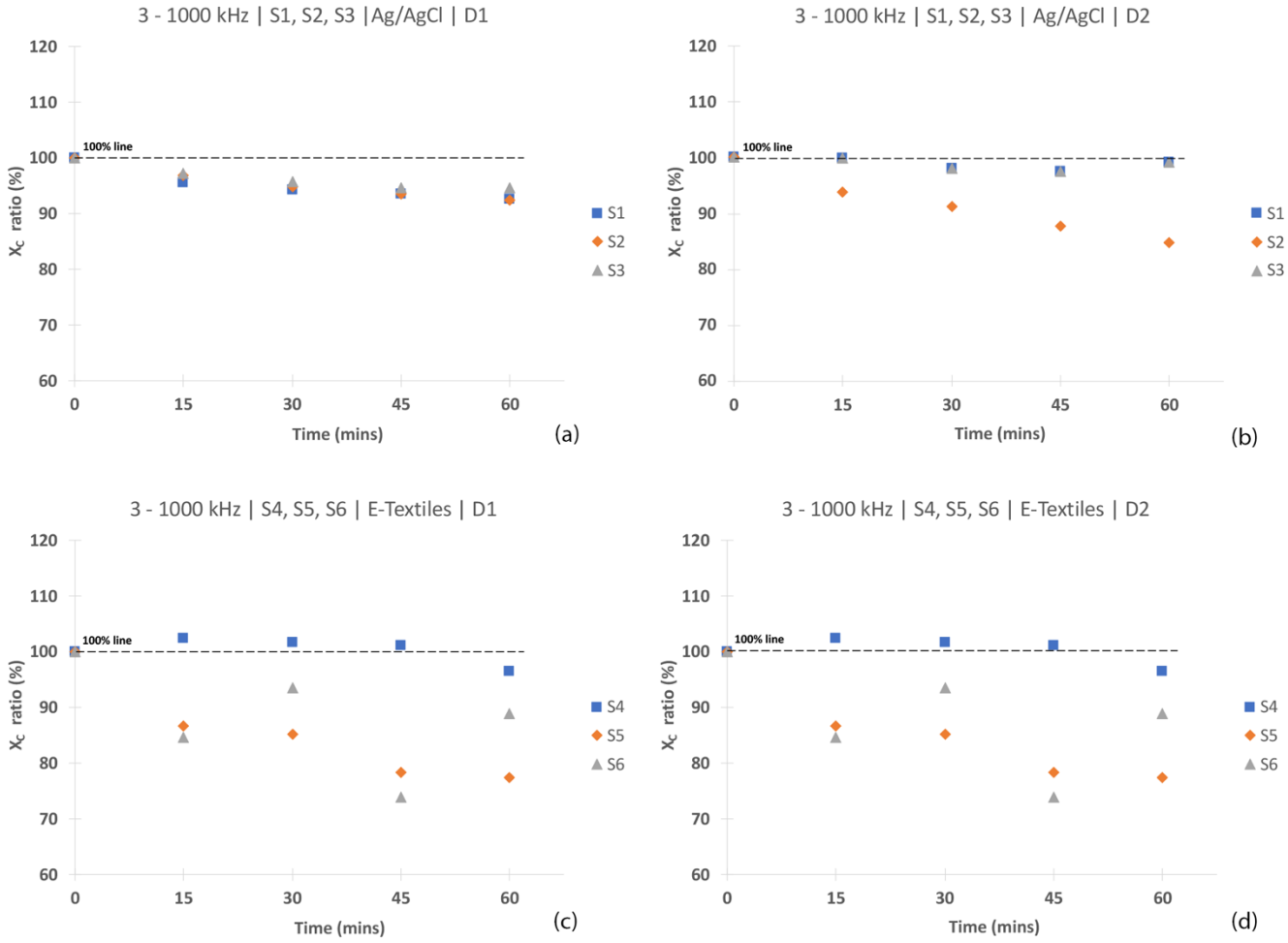

Figure 12. X_C ratio relative to time at 3-1000 kHz sweep for electrodes: (a) Ag/AgCl day 1 and (b) day 2; (c) e-textiles day 1 and (d) day 2.

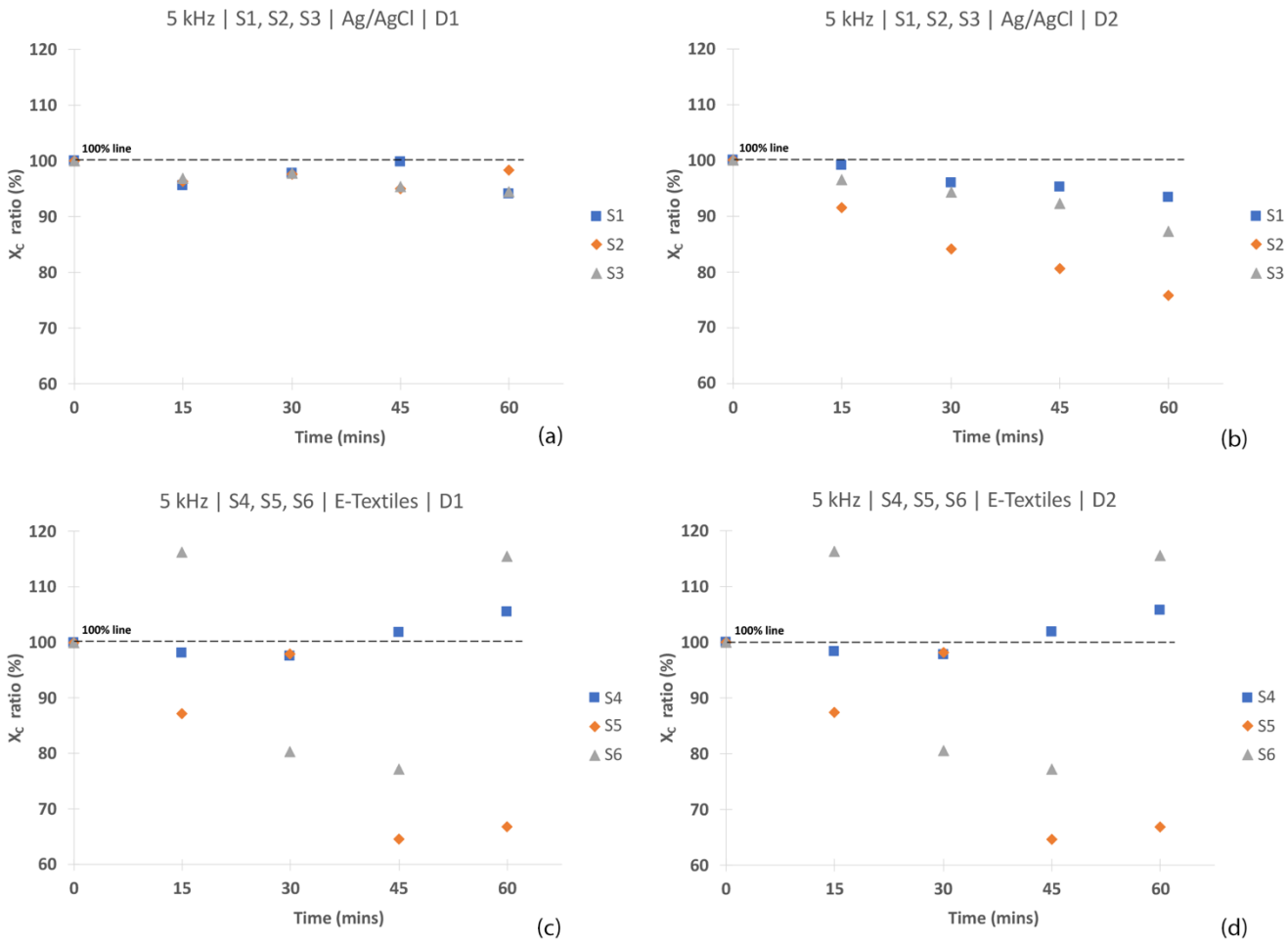

Figure 13. X_C ratio relative to time at 5 kHz for electrodes: (a) Ag/AgCl day 1 and (b) day 2; (c) e-textiles day 1 and (d) day 2.

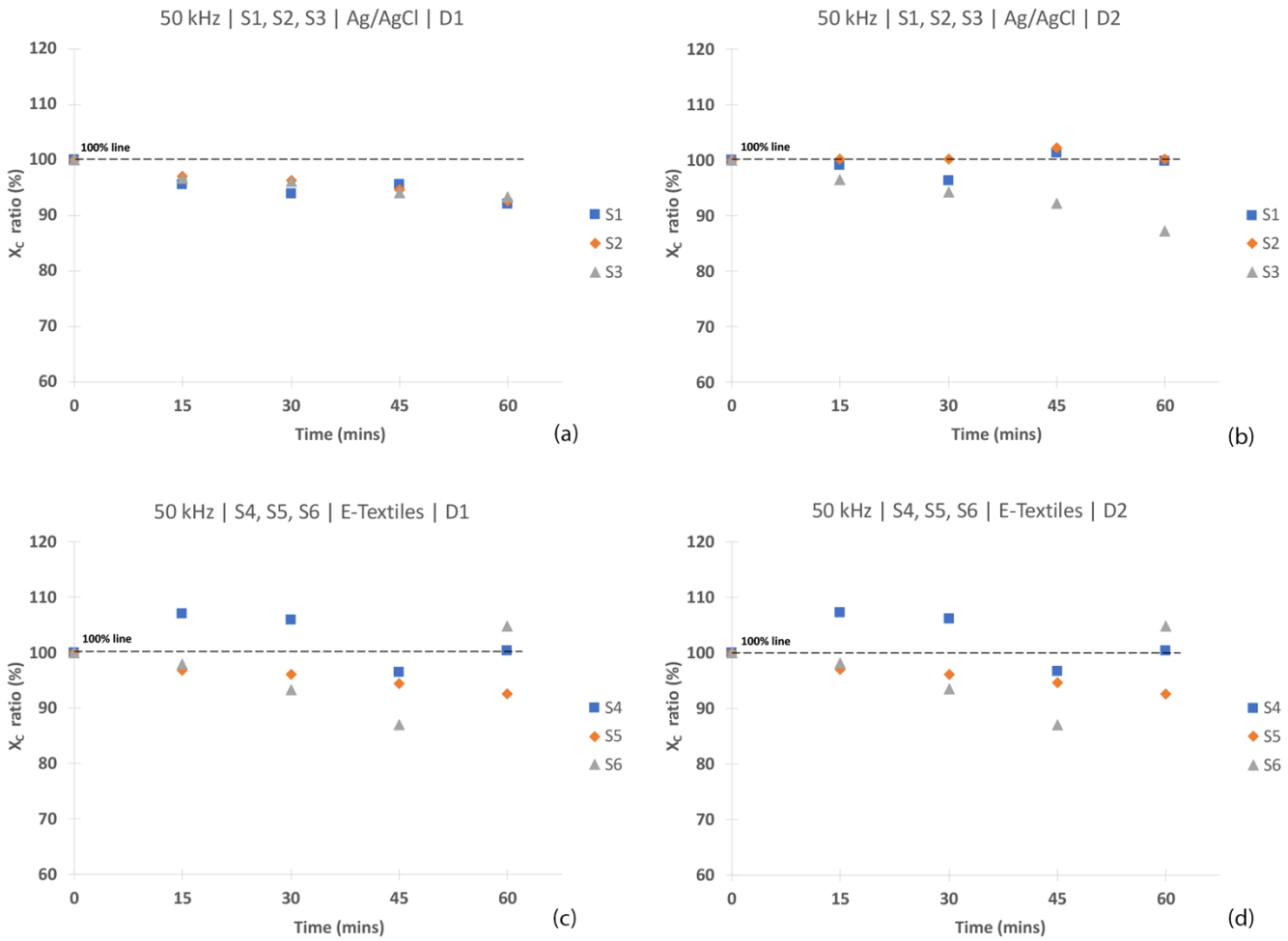

Figure 14. X_C ratio relative to time at 50 kHz for electrodes: (a) Ag/AgCl day 1 and (b) day 2; (c) e-textiles day 1 and (d) day 2.

3.3.4 Evaluation of φ. Referring to Figure 15a-b, the frequency sweep demonstrates a consistent trend for φ associated with the Ag/AgCl electrodes. However, for the discrete frequency at 5 kHz (Figure 16a-b) there is a slight deviation from the 100% line over the two days. An increase in φ over time is observed on day 1 while on day 2 a decrease was noticed. At 50 kHz, day 1 showed stability in φ, while day 2 S2 deviated, refer to Figure 15a-b. Thus, indicating there is a chance of instability adapting φ as a parameter with Ag/AgCl electrodes. Testing the e-textile electrodes was indicative of unstable measurements. Referring to the frequency sweep on day 1, (Figure 15c) all samples (S4-S6) deviated from the 100% line. While day 2, S5 and S6 indicated stability comparable to the Ag/AgCl electrodes; however, S4 demonstrated deviation over time from the 100% line (refer to Figure 15d). By observing the trends associated to φ across the samples and frequency settings, an inconsistency in R^2 was also observed, refer to table 3, Appendix II.

At 5 kHz (Figure 16c-d) the e-textile electrodes demonstrated significant scattering and no discernible trend was observed. Thus, no comparison can be deduced for the two types of electrodes over the two days. However, at 50 kHz only S5 demonstrated stability over the two days and S6 on day 2, Figure 17c-d. Although great variances were observed in R^2 associated to the regression trends. Due to the inconsistency over the two days across the S4-S6, it is safe to assume that washing the e-textile electrodes did not compromise their performance. Given the inconsistency across the BUS samples using Ag/AgCl and e-textile electrode at the discrete frequencies of 5 and 50 kHz, it is possible that this was influenced by any noise present in X_C. This noise is expected to have a greater influence on the e-textile electrodes, refer to figures 15c-d, 16c-d and 17c-d. Thus, no comparison can be made between the Ag/AgCl and e-textile electrodes.

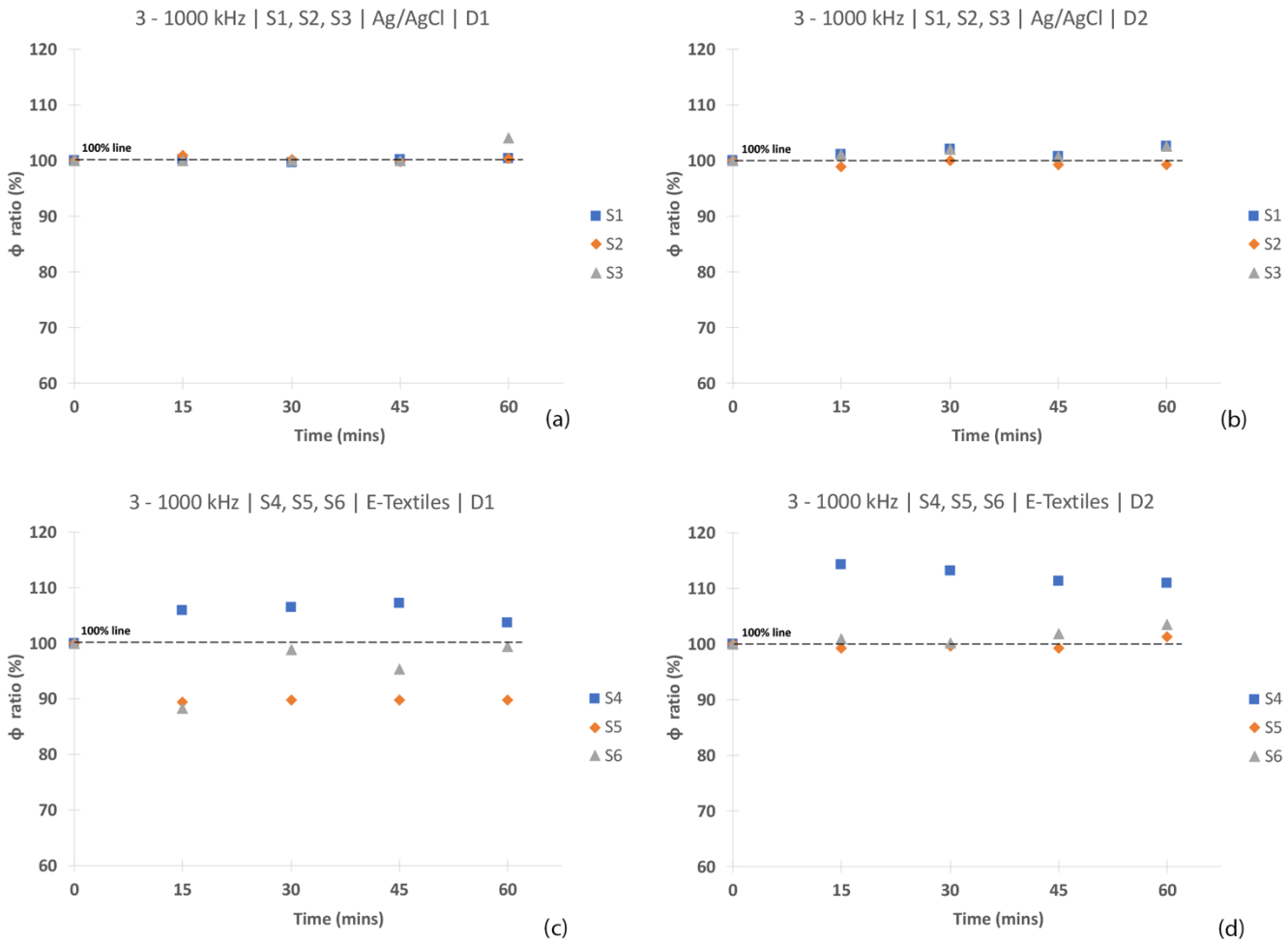

Figure 15. φ ratio relative to time at 3-1000 kHz sweep for electrodes: (a) Ag/AgCl day 1 and (b) day 2; (c) e-textiles day 1 and (d) day 2.

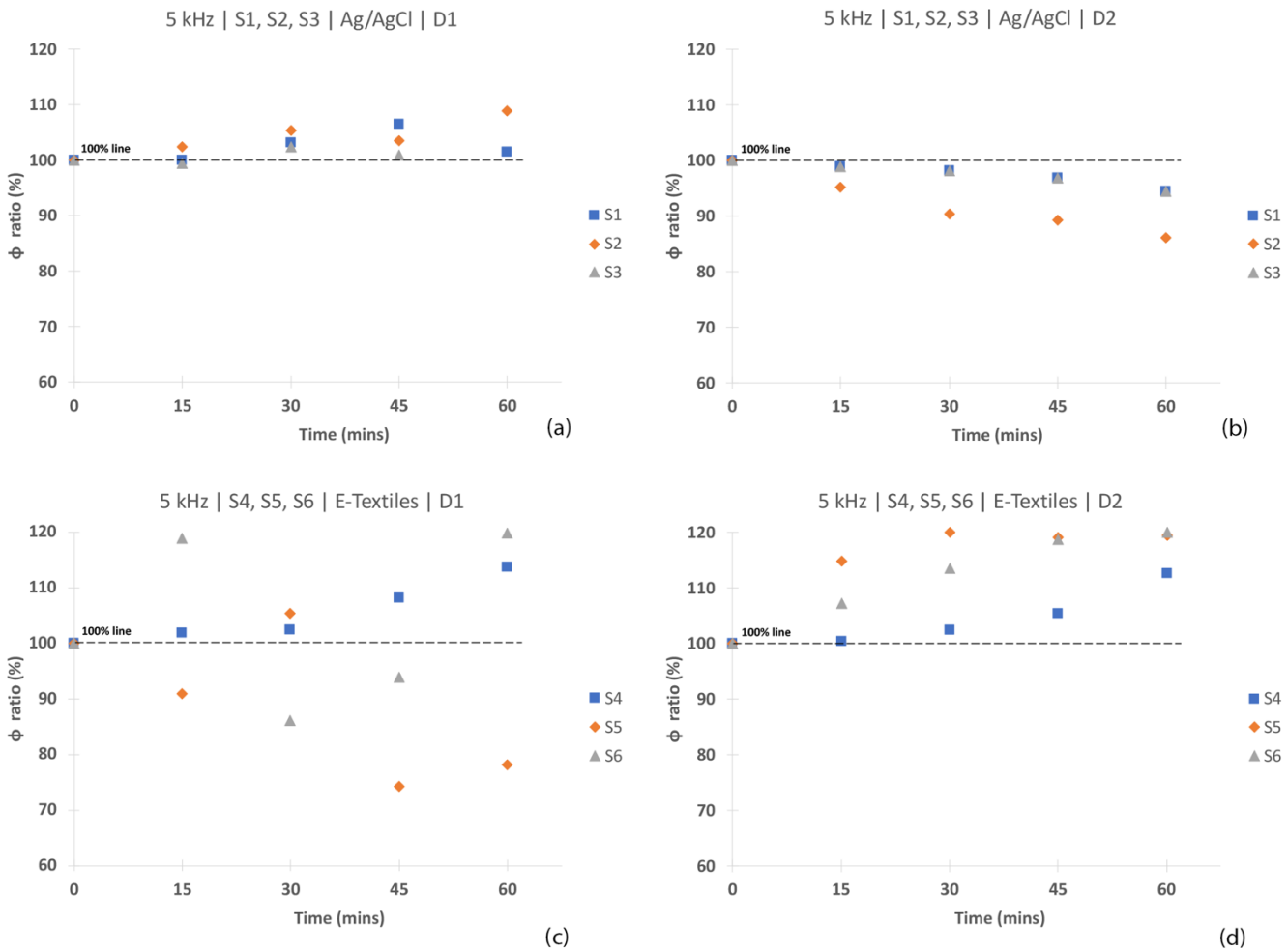

Figure 16. φ ratio relative to time at 5 kHz for electrodes: (a) Ag/AgCl day 1 and (b) day 2; (c) e-textiles day 1 and (d) day 2.

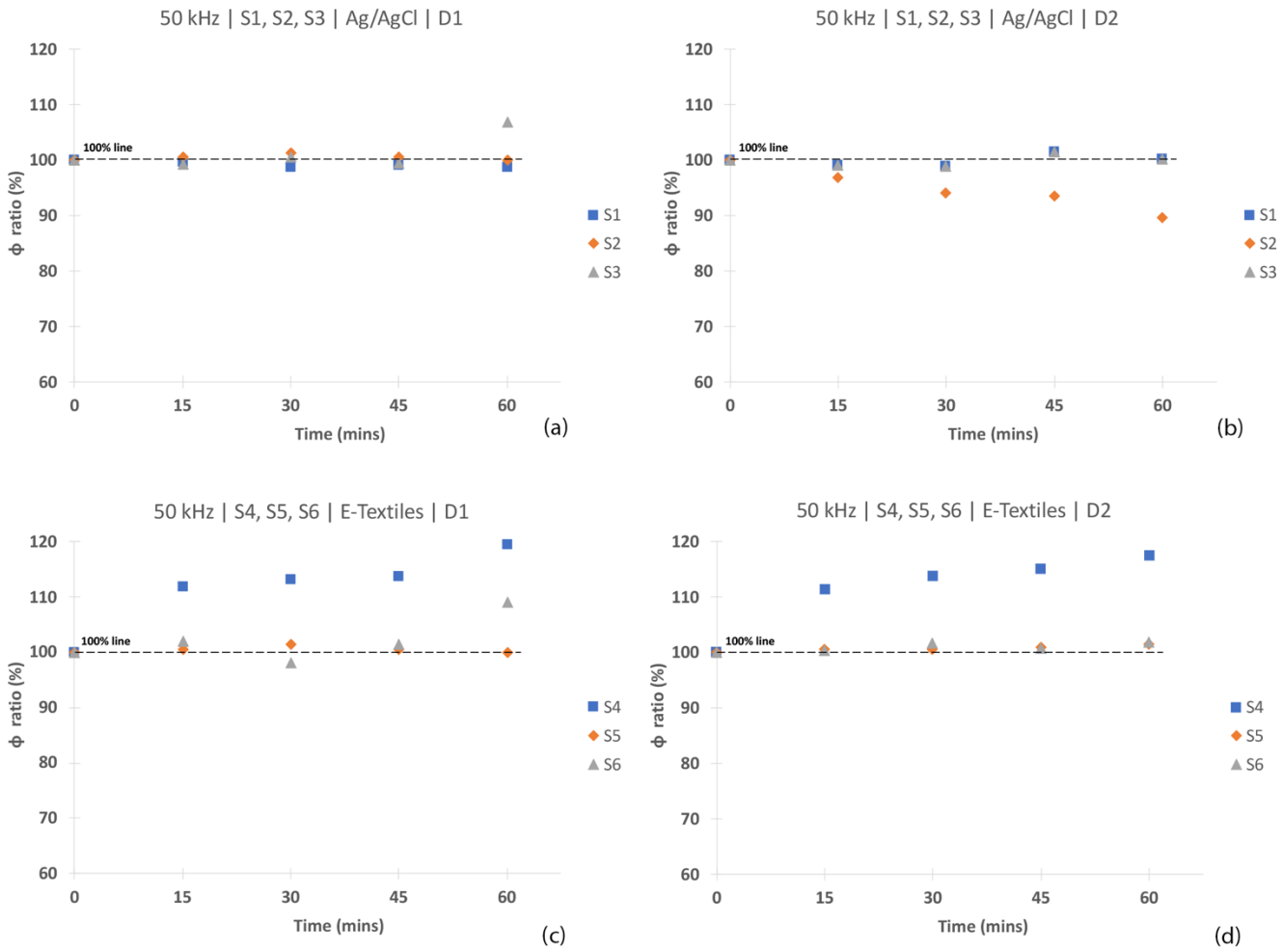

Figure 17. φ ratio relative to time at 50 kHz for electrodes: (a) Ag/AgCl day 1 and (b) day 2; (c) e-textiles day 1 and (d) day 2.

3.3.5 Evaluation of R_0 and R_{inf}. For the parameters R_0 and R_{inf}, a gradual decrease was observed with the samples measured using the Ag/AgCl electrodes, refer to Figure 18a-b and 19a-b. By observing the exponential trend, a strong correlation was observed where $R^2 > 0.85$. However, the e-textile electrodes demonstrated scattering relative to time on day 1 (refer to Figure 18c). On day 2, a defined decrease relative to time was not clearly observed. However, the results were slightly improved from day 1 (Figure 18d). This was also observed in the exponential trend correlation coefficient where on day 1, R^2 ranged between 0.47 – 0.62 and on day 2 R^2 was between 0.42 – 0.81 across the samples, refer to Table 4, Appendix II. R_{inf} clearly demonstrates a decrease relative to time (Figure 19c-d) which can be compared to the Ag/AgCl electrodes. A strong correlation was observed across all samples where $R^2 > 0.88$, refer to Table 5, Appendix II. The parameters R_0 and R_{inf} are determined based on the Cole model adapted to plot an ideal contour to the measurements across the frequency sweep. The significant scattering of X_C relative to time prevalent to the e-textile electrodes would have influenced the Cole model, this potentially impacted the algorithms computing R_0 and R_{inf} associated with the model.

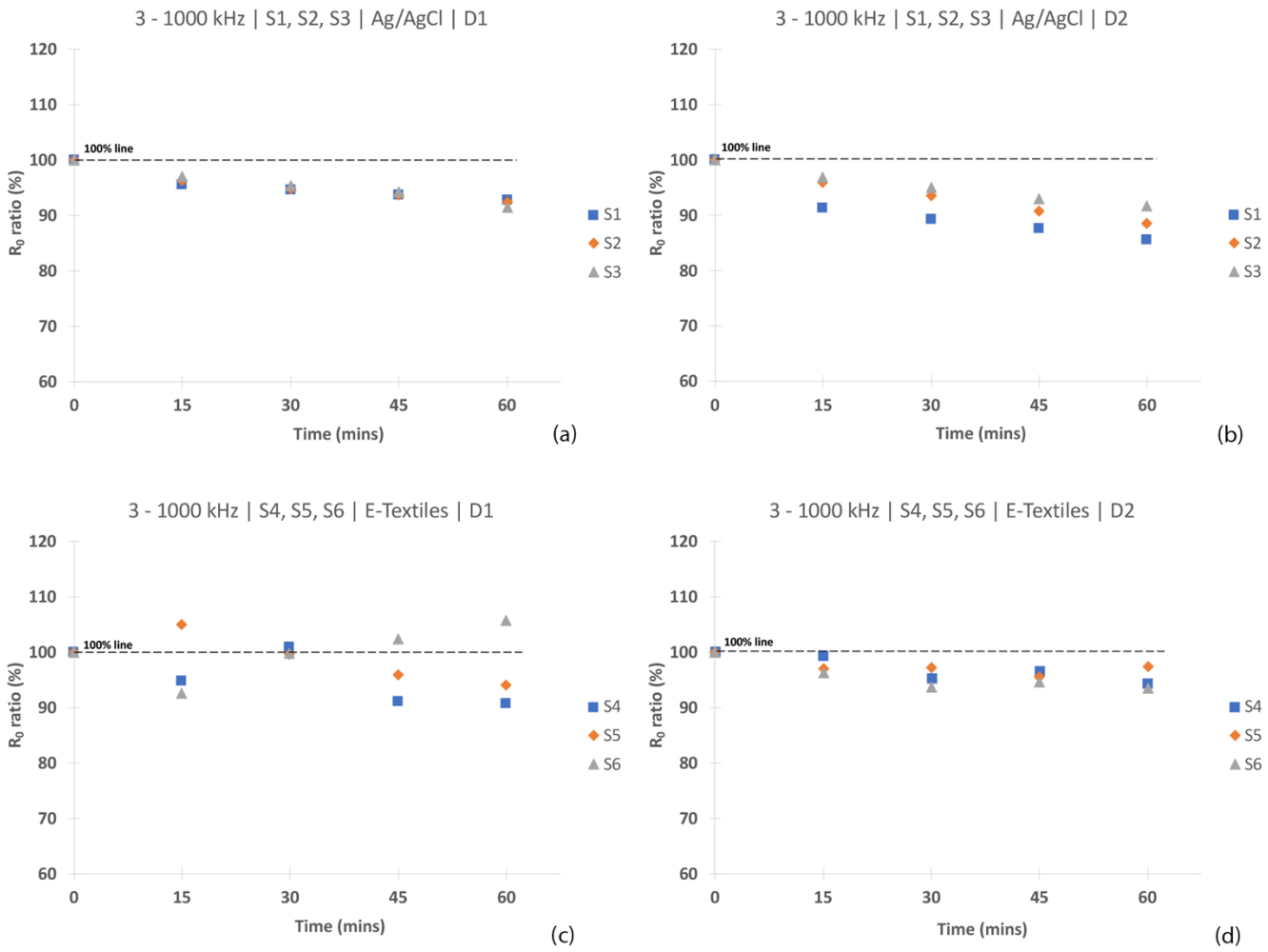

Figure 18. R_0 ratio relative to time at 3-1000 kHz sweep for electrodes: (a) Ag/AgCl day 1 and (b) day 2; (c) e-textiles day 1 and (d) day 2.

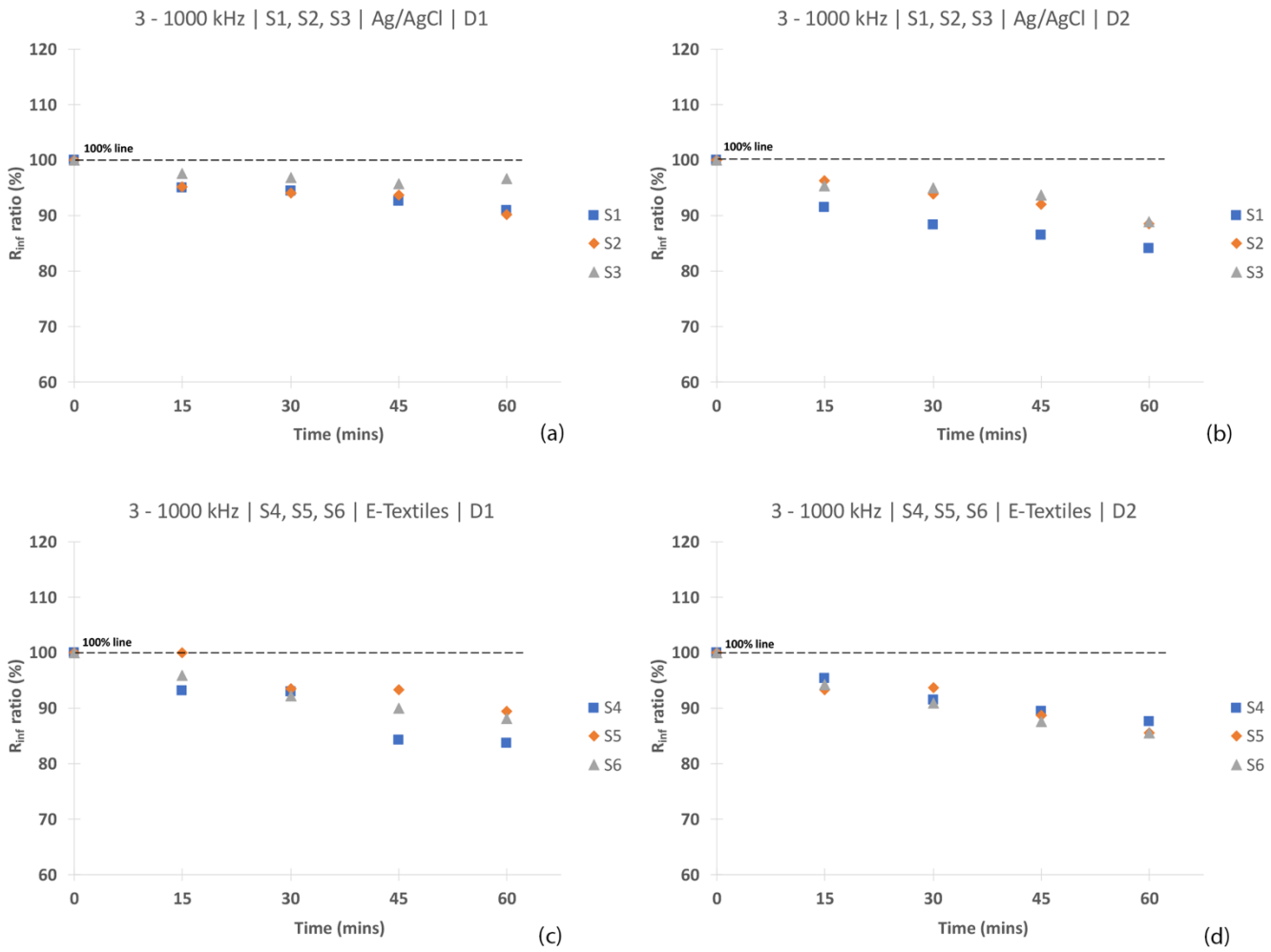

Figure 19. R_{inf} ratio relative to time at 3-1000 kHz sweep for electrodes: (a) Ag/AgCl day 1, (b) day 2; (c) e-textiles day 1, (d) day 2.

4. Discussion

This study was based on current methodologies adapted to measuring wounds using BIA. Pork belly was selected as a BUS to test the e-textile electrodes.

The advantage of pork belly in this study is that is necrotic and there are no biosignals that could potentially influence measurements. However, given that it is meat and testing is conducted in ambient room temperature it has its limitations, specifically time where bacterial growth can spoil the meat [103] thus influencing its electrical properties. The preliminary study conducted in Part B was to determine the trend against time in order to identify its behaviour over time and adjust this variable accordingly in Part C. Measurements were taken by setting up the electrodes in a local configuration using the SFB7. Kenworthy et al. indicates that a local configuration using the SFB7 can be adapted if strict electrode placement protocols are followed for consistency in measurements despite if the devices is designed for whole body configuration [70].

The voltage sensor electrodes were positioned adjacent to an open excision relative to the size of the measured wounds, with a 1 cm distance between the injecting electrodes. For the BUS sample measurements with a frequency sweep (3-1000 kHz) and the discrete frequencies 5 and 50 kHz, an identical trend was observed for the BIA parameters *Z* and *R*. This was demonstrated over two days indicating that by washing the e-textile electrodes, the performance was not compromised. The observed exponential decrease relative to time could potentially be related to decrease associated with necrosis or the water loss from the raw pork [104–107]. Although, some research suggests that an exponential decrease is demonstrated in-vivo before setting over a continuous time period [100,108–110]. However, this study focuses on identifying the use of e-textile electrodes for BIA measurements and the exponential decrease of *Z* is outside of this research.

Research into incorporating dry electrodes for wearable systems report a significantly greater skin-electrode impedance [111] compared to common clinical electrodes associated to systems at significantly lower frequencies.

Although our study does adapt the e-textile electrodes for larger frequencies, an important aspect is the approach of applying the e-textile electrodes to minimise any error. For example, this could be due to the method used in attaching the dry electrodes to the skin. Given that the e-textile electrodes do not have an adhesive layer, this potentially can give rise to an air gap between the electrodes and skin thus increasing Z. By using the heavy weight crepe bandage in the form of a compression sleeve for the two types of electrodes (i.e. the Ag/AgCl and e-textiles), a relatively controlled pressure was applied and the measured impedance values for the e-textile electrodes were of the same magnitude to the Ag/AgCl electrodes. Applying a pressure to electrodes measuring biosignals has demonstrated to improve the performance of wet and dry electrodes [100].

However, a comparison was not observed between the Ag/AgCl and e-textile electrodes for the parameters X_C and φ for the frequency sweep or discrete frequencies 5 and 50 kHz. Although, an identifiable trend was not demonstrated with the Ag/AgCl electrodes for X_C relative to time, a predominant scattering was observed for the e-textile electrodes. Given that the Cole model is dependent on R and X_C, it is expected that this scattering in X_C influences the parameters R_0 and R_{inf}. R_0 was shown to decrease relative to time for the Ag/AgCl electrodes; however, this was not true for the BUS samples measured using the e-textile electrodes. Contrarily, R_{inf} did display a decrease for the types of electrodes (i.e. Ag/AgCl and e-textile electrodes); however, the rate of decrease slightly varied. This could also be dependent upon the BUS samples and not directly related to the electrodes. Although, given that R was comparable between the two types of electrodes in the frequency sweep, it is most likely influenced by the irregularity associated with X_C.

Regarding the irregular performance of the e-textile electrodes when measuring φ, this could also be closely associated to the noise impacting X_C. Research into φ using standard Ag/AgCl electrodes suggest that φ cannot be associated to the Cole model due to the anisotropic nature of skin [112]. This was also demonstrated at the discrete frequencies of 5 and 50 kHz. It is safe to assume that X_C was influenced by external noise. Although a tetrapolar configuration is preferred to reduce interferences [113], recent research suggests that a tetrapolar configuration is also susceptible to noise [98]. This noise could potentially be associated to the electrode-skin interface. However, this was not evident in the signal given that the actual measurements defined and adapted for the algorithm of the Cole plots across all measurements did not indicate any interference.

E-textile electrodes have capacitance properties contrary to Ag/AgCl electrodes [97]. For the frequencies adapted in BIA (i.e. ranging between 3-1000 kHz inclusive of the discrete frequencies), the absolute values for X_C are relatively small compared to R. This can be observed by the direct relation of Z and R. The equivalent capacitor values measured at 50 kHz, indicated a coupling capacitance of magnitude in the μF range. Therefore, from this it is safe to assume that it is more susceptible to noise. This can also be said for the Ag/AgCl electrodes in-vivo [114]. In ECG measurements in-vivo, it has been shown that the capacitance properties of the skin-electrode impedance is inconsistent contrary to its resistive properties [115].

In addition to the equipment, there is also the microclimate of the electrodes that can influence their performance. For example, given that the electrodes are secured with a compression sleeve, this microclimate formed by the sleeve can influence the performance of the Ag/AgCl and e-textile electrodes [116]. This microclimate can potentially be unstable relative to time thus impacting X_C. This can be related to the influence of the relative humidity [117]. Our previous research indicated that the relative humidity was associated to a change in the polarization impedance of e-textile electrodes [58,87]. However, given that the Ag/AgCl electrodes are considered ideally non-polarized, it is safe to assume that they are less susceptible to changes in relative humidity.

Another impacting factor could be associated with the electrode-skin interface. This could be due to lipids of skin or the inhomogeneity of both the skin and electrode surface. Research suggests that certain lipid bilayers found on the surface of the skin have capacitance properties causing a barrier against the penetration of charge [112]. Given that the Ag/AgCl electrodes possess an electrolyte gel layer enhancing the redox reaction, this could assist in counteracting the lipid bilayers allowing easier penetration of the charge in comparison to the e-textile electrodes. Another concern with the electrode-skin contact is the nature of the conductive interface surface of the e-textile electrodes [118]. Given that it has a rougher surface in comparison to the Ag/AgCl adhesive surface, this could cause a non-uniform charge density on the surface. This, in addition to the non-uniform nature of skin due to its sulci, could result in a loss of charge between the electrode-skin interface. This may have less impact on the Ag/AgCl electrodes due to its adhesive layer reducing any air gaps thus improving the charge penetration. Improvement of Z_{es} could be expected when using e-textile electrodes on living skin, due to perspiration which will fill the air gaps at the electrode-skin interface.

Our study demonstrates that e-textile electrodes can be adapted to measure Z and R associated with BIA to monitor wound healing in a local tetrapolar configuration. It is also shown that by washing the e-textile electrodes, their efficacy was not compromised. Their trend relative to time is comparable to common clinical Ag/AgCl electrodes. However, it is important to take into consideration that they are not as reliable as Ag/AgCl when measuring X_C and φ. This is demonstrated for a frequency sweep of 3-1000 kHz and the discrete frequencies 5 and 50 kHz common in BIA

measurements. The e-textile electrodes were also found to not be as reliable as the Ag/AgCl electrodes when measuring R_0; however, they did indicate a decrease relative to time for R_{inf} as demonstrated by the Ag/AgCl electrodes. To adapt e-textile electrodes for BIA systems to improve their efficacy in measuring X_C, φ and R_0, additional front-end hardware can be designed and adapted reducing any potential noise.

5. Conclusion

Research in monitoring wounds adapting BIA systems that use a frequency sweep or discrete frequency focus on trends associated to the parameters Z, R, X_C, φ, R_0 and R_{inf}. These studies are based on static measurements on a day to day basis. By adapting e-textile electrodes to monitor wounds, dynamic long-term monitoring of wounds can be studied without the need of replacing Ag/AgCl electrodes due to degradation. Research that dynamically monitors a wound has yet to be conducted. The degradation of wet electrodes would require a regular change of electrodes; therefore, this could have an influence on the results. The performance of the e-textile electrodes ex-vivo indicate that they are comparable to Ag/AgCl when measuring Z and R over a 60-minute period. Future research into the efficacy of e-textile electrodes for BIA applications measuring Z can be conducted in-vivo and compared to Ag/AgCl on undamaged skin. Moreover, with the development a wearable system that adapts dynamic monitoring functionality while incorporating a calibrating system for e-textile electrodes, continuous monitoring of wounds relative to time can be measured. This can provide further insight into the wound healing process through measuring Z while any complications to the wound can be determined at an early stage. By determining the onset of any complications in the wound healing process early, appropriate treatment can be administered thus reducing the risk of the patient suffering from infections that can potentially lead to amputation.

Acknowledgements

I would like to thank Elena Pirogova and Peter Dabnicki for providing lab access and lab assistance.

References

[1] Drew P, Posnett J and Rusling L 2007 The cost of wound care for a local population in England *Int. Wound J.* **4** 149–55

[2] Mcisaac C 2005 Managing wound care outcomes *Ostomy. Wound. Manage.* **51** 54–9

[3] Hjort A and Gottrup F 2010 Cost of wound treatment to increase significantly in Denmark over the next decade *J. Wound Care* **19** 173-174,176,178,180,182,184

[4] Fife C, Carter M, Walker D and Thomson B 2012 Wound care outcomes and associated cost among patients treated in US outpatient wound centers: Data from the US wound registry *Wounds* **24** 10–7

[5] Anon Standards for wound prevention and management (Third Edition) (2016)

[6] Sood A, Granick M S, Trial C, Lano J, Palmier S, Ribal E and Téot L 2016 The role of telemedicine in wound care: A review and analysis of a database of 5,795 patients from a mobile wound-healing center in Languedoc-Roussillon, France *Plast. Reconstr. Surg.* **138** 248S-256S

[7] Jayachandran M, Rodriguez S, Solis E, Lei J and Godavarty A 2016 Critical review of noninvasive optical technologies for wound imaging *Adv. Wound Care* **5**

[8] Kooner S, Sheehan B, Kendal J and Johal H 2018 Development of a simple multidisciplinary arthroplasty wound-assessment instrument: the SMArt Wound Tool *Can. J. Surg.* **61** 326–31

[9] Lucas Y and Treuillet S 2018 Optical imaging technology for wound assessment: A state of the art *Lect. Notes Comput. Vis. Biomech.* **27** 745–53

[10] Langemo D and Spahn J 2016 A multimodality imaging and software system for combining an anatomical and physiological assessment of skin and underlying tissue conditions *Adv. Skin Wound Care* **29** 155–63

[11] Mchugh M J 2016 Wound metrology: Strategies for achieving accuracy in wound measurement *Wounds UK* **12** 20–5

[12] Lee J, Kim D, Ryoo H-Y and Shin B-S 2016 Sustainable wearables: Wearable technology for enhancing the quality of human life *Sustainability* **8** 466

[13] Cheung M L, Chau K Y, Lam M H S, Tse G, Ho K Y, Flint S W, Broom D R, Tso E K H and Lee K Y 2019 Examining consumers' adoption of wearable healthcare technology: The role of health attributes *Int. J. Environ. Res. Public Health* **16** 2257

[14] Logothetis I, Matsouka D, Vassiliadis S, Vossou C and Siores E 2018 Optimum operating conditions for PZT actuators for vibrotactile wearables *J. Electron. Mater.* **47** 3709–16

[15] Albulbul A 2016 Evaluating major electrode types for idle biological signal measurements for modern medical technology *Bioengineering* **3** 20

[16] Huigen E, Peper A and Grimbergen C A 2002 Investigation into the origin of the noise of surface electrodes *Med. Biol. Eng. Comput* **40** 332–8

[17] McAdams E, Jossinet J, Lackermeier A and Risacher F 1996 Factors affecting electrode-gel-skin interface impedance in electrical impedance tomography *Med. Biol. Eng. Comput.* **34** 397–408

[18] Logothetis I, Fernandez-Garcia R, Troynikov O, Dabnichki P, Pirogova E and Gil I 2019 Embroidered electrodes for bioelectrical impedance analysis: impact of surface area and stitch parameters *Meas. Sci. Technol.* **30** 115103

[19] Freeborn T, Crenshaw T and Critcher S 2017 Hook

artifact correction of localized electrical bioimpedance for improved agreement between different device measurements *Biomed. Phys. Eng. Express* **4**

[20] Bogónez-Franco P, Pham P, Gehin C, Massot B, Delhomme G, Guillemaud R and McAdams E 2014 *Effect of electrode contact impedance mismatch on 4-electrode measurements of small body segments using commercial BIA devices*

[21] Kaappa E S, Joutsen A, Cömert A and Vanhala J 2017 The electrical impedance measurements of dry electrode materials for the ECG measuring after repeated washing *Res. J. Text. Appar.* **21** 59–71

[22] Li G, Lyu X, Wang Z, Rong Y, Hu R, Luo Z and Wang Y 2017 All-solid-state carbonate-selective electrode based on screen-printed carbon paste electrode *Meas. Sci. Technol.* **28** 025104

[23] Peng H L, Liu J Q, Dong Y Z, Yang B, Chen X and Yang C S 2016 Parylene-based flexible dry electrode for bioptential recording *Sensors Actuators, B Chem.* **231** 1–11

[24] Khan Y, Pavinatto F J, Lin M C, Liao A, Swisher S L, Mann K, Subramanian V, Maharbiz M M and Arias A C 2016 Inkjet-printed flexible gold electrode arrays for bioelectronic interfaces *Adv. Funct. Mater.* **26** 1004–13

[25] Schnitker J, Adly N, Seyock S, Bachmann B, Yakushenko A, Wolfrum B and Offenhäusser A 2018 Rapid prototyping of ultralow-cost, inkjet-printed carbon microelectrodes for flexible bioelectronic devices *Adv. Biosyst.* **2** 1700136

[26] Lee J W and Yun K S 2017 ECG monitoring garment using conductive carbon paste for reduced motion artifacts *Polymers (Basel).* **9** 439

[27] Kabiri Ameri S, Ho R, Jang H, Tao L, Wang Y, Wang L, Schnyer D M, Akinwande D and Lu N 2017 Graphene electronic tattoo sensors *ACS Nano* **11** 7634–41

[28] Bareket L, Inzelberg L, Rand D, David-Pur M, Rabinovich D, Brandes B and Hanein Y 2016 Temporary-tattoo for long-term high fidelity biopotential recordings *Sci. Rep.* **6** 25727

[29] Posada-Quintero H, Noh Y, Eaton-Robb C, Florian J P and Chon K H 2018 Feasibility Testing of Hydrophobic Carbon Electrodes for Acquisition of Underwater Surface Electromyography Data *Ann. Biomed. Eng.* **46** 1397–405

[30] Jung H C, Moon J H, Baek D H, Lee J H, Choi Y Y, Hong J S and Lee S H 2012 CNT/PDMS composite flexible dry electrodesfor long-term ECG monitoring *IEEE Trans. Biomed. Eng.* **59** 1472–9

[31] Kim T, Park J, Sohn J, Cho D and Jeon S 2016 Bioinspired, highly stretchable, and conductive dry adhesives based on 1D-2D hybrid carbon nanocomposites for all-in-one ECG electrodes *ACS Nano* **10** 4770–8

[32] Lee S M, Byeon H J, Lee J H, Baek D H, Lee K H, Hong J S and Lee S H 2014 Self-adhesive epidermal carbon nanotube electronics for tether-free long-term continuous recording of biosignals *Sci. Rep.* **4** 1–9

[33] Liu B, Luo Z, Zhang W, Tu Q and Jin X 2016 Silver nanowire-composite electrodes for long-term electrocardiogram measurements *Sensors Actuators, A Phys.* **247** 459–64

[34] Liu B, Luo Z, Zhang W, Tu Q and Jin X 2016 Carbon nanotube-based self-adhesive polymer electrodes for wireless long-term recording of electrocardiogram signals *J. Biomater. Sci. Polym. Ed.* **27** 1899–908

[35] Zhao Y, Cao Y, Liu J, Zhan Z, Li X and Li W 2018 Single-wall carbon nanotube-coated cotton yarn for electrocardiography transmission *Micromachines* **9** 132

[36] Imani S, Bandodkar A J, Mohan A M V, Kumar R, Yu S, Wang J and Mercier P P 2016 A wearable chemical-electrophysiological hybrid biosensing system for real-time health and fitness monitoring *Nat. Commun.* **7** 1–7

[37] Yapici M K, Alkhidir T, Samad Y A and Liao K 2015 Graphene-clad textile electrodes for electrocardiogram monitoring *Sensors Actuators, B Chem.* **221** 1469–74

[38] Yapici M K and Alkhidir T E 2017 Intelligent medical garments with graphene-functionalized smart-cloth ECG sensors *Sensors (Switzerland)* **17**

[39] Shafti A, Manero R B R, Borg A M, Althoefer K and Howard M J 2016 Designing embroidered electrodes for wearable surface electromyography *Proceedings - IEEE International Conference on Robotics and Automation* vol 2016-June (Institute of Electrical and Electronics Engineers Inc.) pp 172–7

[40] Trindade I, Spranger P, Martins F, Miguel R and Silva M 2014 Fully integrated embroidery process for smart textiles *Tech. Proc. 2014 NSTI Nanotechnol. Conf. Expo, NSTI-Nanotech 2014* **3** 65–8

[41] Trindade I, Machado da Silva J, Miguel R, Pereira M, Lucas J, Oliveira L, Valentim B, Barreto J and Santos Silva M 2016 Design and evaluation of novel textile wearable systems for the surveillance of vital signals *Sensors* **16** 1573

[42] Weder M, Hegemann D, Amberg M, Hess M, Boesel L, Abächerli R, Meyer V and Rossi R 2015 Embroidered electrode with silver/titanium coating for long-term ECG monitoring *Sensors* **15** 1750–9

[43] Cho G, Jeong K, Paik M J, Kwun Y and Sung M 2011 Performance evaluation of textile-based electrodes and motion sensors for smart clothing *IEEE Sens. J.* **11** 3183–93

[44] Guo X, Huang Y, Cai X, Liu C and Liu P 2016 Capacitive wearable tactile sensor based on smart textile substrate with carbon black /silicone rubber composite dielectric *Meas. Sci. Technol.* **27** 45105

[45] Haddad P, Servati A, Soltanian S, Ko F and Servati P 2018 Breathable Dry Silver/Silver Chloride Electronic Textile Electrodes for Electrodermal Activity Monitoring *Biosensors* **8** 79

[46] Bihar E, Roberts T, Ismailova E, Saadaoui M, Isik M,

Sanchez-Sanchez A, Mecerreyes D, Hervé T, De Graaf J B and Malliaras G G 2017 Fully printed electrodes on stretchable textiles for long-term electrophysiology *Adv. Mater. Technol.* **2** 1600251

[47] Takamatsu S, Lonjaret T, Crisp D, Badier J M, Malliaras G G and Ismailova E 2015 Direct patterning of organic conductors on knitted textiles for long-term electrocardiography *Sci. Rep.* **5** 1–7

[48] Karim N, Afroj S, Malandraki A, Butterworth S, Beach C, Rigout M, Novoselov K S, Casson A J and Yeates S G 2017 All inkjet-printed graphene-based conductive patterns for wearable e-textile applications *J. Mater. Chem. C* **5** 11640–8

[49] Paul G, Torah R, Beeby S and Tudor J 2017 A printed, dry electrode Frank configuration vest for ambulatory vectorcardiographic monitoring *Smart Mater. Struct.* **26** 025029

[50] Sinha S K, Noh Y, Reljin N, Treich G M, Hajeb-Mohammadalipour S, Guo Y, Chon K H and Sotzing G A 2017 Screen-printed PEDOT:PSS electrodes on commercial finished textiles for electrocardiography *ACS Appl. Mater. Interfaces* **9** 37524–8

[51] Pani D, Dessi A, Saenz-Cogollo J F, Barabino G, Fraboni B and Bonfiglio A 2016 Fully Textile, PEDOT:PSS Based Electrodes for Wearable ECG Monitoring Systems *IEEE Trans. Biomed. Eng.* **63** 540–9

[52] Beckmann L, Neuhaus C, Medrano G, Jungbecker N, Walter M, Gries T and Leonhardt S 2010 Characterization of textile electrodes and conductors using standardized measurement setups *Physiol. Meas.* **31** 233–47

[53] Goncu Berk G 2018 Design of a wearable pain management system with embroidered TENS electrodes *Int. J. Cloth. Sci. Technol.* **30** 38–48

[54] Kalvøy H 2011 New method for separation of electrode polarization impedance from measured tissue impedance *Open Biomed. Eng. J.* **5** 8–13

[55] Hao L and Xiaoming T 2015 Evaluation methods and instruments of dry biopotential electrodes *Handbook of Smart Textiles* ed T Xiaoming (Springer) pp 775–808

[56] Taji B, Chan A D C and Shirmohammadi S 2018 Effect of pressure on skin-electrode impedance in wearable biomedical measurement devices *IEEE Trans. Instrum. Meas.* **67** 1900–12

[57] Yao S and Zhu Y 2016 Nanomaterial-enabled dry electrodes for electrophysiological sensing: A review *JOM* **68** 1145–55

[58] Logothetis I, Vatansever Bayramol D, Gil I, Dabnichki P and Pirogova E 2020 Evaluating silver-plated nylon (Ag/PA66) e-textiles for bioelectrical impedance analysis (BIA) application *Meas. Sci. Technol.* **31** 75101

[59] Spach M S, Barr R C, Havstad J W and Long E C 1966 Skin-electrode impedance and its effect on recording cardiac potentials *Circulation* **34** 649–56

[60] Berson A S and Pipberger H V. 1968 Skin-electrode impedance problems in electrocardiography *Am. Heart J.* **76** 514–25

[61] Muller M, Cristante J, Foote A, Montalibet A, Gharbi S, McAdams E and Pham P 2015 The use of multi-frequency impedimetry for the monitoring of chronic wounds: the BIPPED clinical study *Proceedings of the 5th EAI International Conference on Wireless Mobile Communication and Healthcare - "Transforming healthcare through innovations in mobile and wireless technologies"* (ICST)

[62] Lukaski H C and Moore M 2012 Bioelectrical impedance assessment of wound healing *J. Diabetes Sci. Technol.* **6** 209–12

[63] Kekonen A, Bergelin M, Eriksson J-E, Ylänen H and Viik J 2015 A quantitative method for monitoring wound healing *Int. J. Bioelectromagn.* **17** 36–41

[64] Prakash S, Karnes M P, Sequin E K, West J D, Hitchcock C L, Nichols S D, Bloomston M, Abdel-Misih S R, Schmidt C R, Martin E W, Povoski S P and Subramaniam V V 2015 Ex vivoelectrical impedance measurements on excised hepatic tissue from human patients with metastatic colorectal cancer *Physiol. Meas.* **36** 315–28

[65] Adler A and Boyle A 2017 Electrical impedance tomography: Tissue properties to image measures *IEEE Trans. Biomed. Eng.* **64** 2494–504

[66] Dowrick T, Blochet C and Holder D 2015 In vivobioimpedance measurement of healthy and ischaemic rat brain: implications for stroke imaging using electrical impedance tomography *Physiol. Meas.* **36** 1273–82

[67] Sanchez B and Rutkove S B 2017 Electrical impedance myography and its applications in neuromuscular disorders *Neurotherapeutics* **14** 107–18

[68] Moncada M E and de la Cruz J 2011 La actividad electrodérmica -Revisión *Ing. e Investig.* **31** 143–51

[69] Brantlov S, Ward L C, Jødal L, Rittig S and Lange A 2017 Critical factors and their impact on bioelectrical impedance analysis in children: a review *J. Med. Eng. Technol.* **41** 22–35

[70] Kenworthy P, Grisbrook T L, Phillips M, Gittings P, Wood F M, Gibson W and Edgar D W 2017 Bioimpedance spectroscopy: A technique to monitor interventions for swelling in minor burns *Burns* **43** 1725–35

[71] Kenworthy P, Phillips M, Grisbrook T L, Gibson W, Wood F M and Edgar D W 2018 Monitoring wound healing in minor burns - A novel approach *Burns* **44** 70–6

[72] Nescolarde L, Yanguas J, Lukaski H, Alomar X, Rosell X and Rodas G 2013 Localized bioimpedance to assess muscle injury *Physiol. Meas.* **34** 237–45

[73] Nescolarde L, Yanguas J, Lukaski H, Alomar X, Rosell-Ferrer J and Rodas G 2014 Effects of muscle injury severity on localized bioimpedance measurements *Physiol. Meas.* **36** 27–42

[74] Nescolarde L, Yanguas J, Terricabras J, Lukaski H,

Alomar X, Rosell X and Rodas G 2017 Detection of muscle gap by L-BIA in muscle injuries: Clinical prognosis *Physiol. Meas.* **38** L1–9

[75] Bartels E M, Sørensen E R and Harrison A P 2015 Multi-frequency bioimpedance in human muscle assessment *Physiol. Rep.* **3** e12354

[76] Macdonald J R and Johnson W B 2005 Fundamentals of impedance spectroscopy *Impedance Spectroscopy* (Wiley) pp 1–26

[77] McAdams E T and Jossinet J 1995 Tissue impedance: A historical overview *Physiol. Meas.* **16** A1

[78] Martinsen Ø G, Grimnes S and Schwan H P 2002 Interface phenomena and dielectric properties of biological tissue *Encyclopedia of surface and colloid science* (New York: Marcel Dekker)

[79] Kenworthy P, Grisbrook T, Phillips M, Gibson W, Wood F and Edgar D 2017 Addressing the barriers to bioimpedance spectroscopy use in major burns: Alternate electrode placement *J. Burn Care Res.* **38** 1

[80] Kekonen A, Bergelin M, Erikssen J E, Kaartinen I and Viik J 2017 Method for evaluation of surgical wound healing: A case study *IFMBE Proceedings* vol 65 (Springer Verlag) pp 446–9

[81] Kekonen A, Bergelin M, Eriksson J E, Ylanen H, Kielosto S and Viik J 2016 Bioimpedance measurement system for evaluation of the status of wound healing *Proceedings of the Biennial Baltic Electronics Conference, BEC* vol 2016-November (IEEE Computer Society) pp 175–8

[82] Kekonen A, Bergelin M, Eriksson J E, Vesa M, Johansson M and Viik J 2019 Long-term monitoring of acute wound healing from beneath the primary wound dressings *Proceedings of the Biennial Baltic Electronics Conference, BEC* vol 2018-October (IEEE Computer Society)

[83] Kekonen A, Bergelin M, Eriksson J-E, Vaalasti A, Ylänen H and Viik J 2017 Bioimpedance measurement based evaluation of wound healing *Physiol. Meas.* **38** 1373–83

[84] King R J, Clamp J A, Hutchinson J W and Moran C G 2007 Bioelectrical impedance: A new method for measuring post-traumatic swelling *J. Orthop. Trauma* **21** 462–8

[85] Landén N X, Li D and Ståhle M 2016 Transition from inflammation to proliferation: a critical step during wound healing *Cell. Mol. Life Sci.* **73** 3861–85

[86] Gonzalez-Correa C A, Rivera-Garzón R A and Martínez-Táutiva S 2019 Electric impedance and the healing of diabetic foot ulcers *J. Phys. Conf. Ser.* **1272** 12009

[87] Logothetis I, Gil I, Dabnichki P and Pirogova E Australian Biomedical Engineering Conference 2019 (ABEC 2019): Technology & Research in Australian Medical Science - E-textiles for bioelectrical impedance analysis (BIA) (Engineering Collection) - Informit

[88] DICK I P and SCOTT R C 1992 Pig ear skin as an in-vitro model for human skin permeability *J. Pharm. Pharmacol.* **44** 640–5

[89] Sains P, Chana K S, Sridhar V and Sajid M S 2018 Pilot study on an innovative biosensor with a range of medical and surgical applications *BMC Res. Notes* **11** 81

[90] Anon Ambu® WhiteSensor WS

[91] Nescolarde L, Lukaski H, De Lorenzo A, De-Mateo-Silleras B, Redondo-Del-Río M P and Camina-Martín M A 2016 Different displacement of bioimpedance vector due to Ag/AgCl electrode effect *Eur. J. Clin. Nutr.* **70** 1401–7

[92] Yamamoto T and Yamamoto Y 1976 Electrical properties of the epidermal stratum corneum *Med. Biol. Eng.* **14** 151–8

[93] Gómez-Snchez J A, Aristizbal-Botero W, Barragn-Arango P J and Felice C J 2009 Introduction of a muscular bidirectional electrical anisotropy index to quantify the structural modifications during aging in raw meat *Meas. Sci. Technol.* **20** 075702

[94] Cömert A, Honkala M and Hyttinen J 2013 Effect of pressure and padding on motion artifact of textile electrodes *Biomed. Eng. Online* **12** 26

[95] Khodasevych I, Parmar S and Troynikov O 2017 Flexible sensors for pressure therapy: Effect of substrate curvature and stiffness on sensor performance *Sensors* **17** 2399

[96] Bai X, Hou J, Wang L, Wang M, Wang X, Wu C, Yu L, Yang J, Leng Y and Sun Y 2018 Electrical impedance analysis of pork tissues during storage *J. Food Meas. Charact.* **12** 164–72

[97] Lee S and Kruse J 2008 Biopotential electrode sensors in ECG/EEG/EMG systems *Analog Devices*

[98] Areny R P 2018 *Tetrapolar bioimpedance measurements compared to four-wire resistance measurements* vol 9

[99] Pola T and Vanhala J 2007 Textile electrodes in ECG measurement *Proceedings of the 2007 International Conference on Intelligent Sensors, Sensor Networks and Information Processing, ISSNIP* pp 635–9

[100] Searle A and Kirkup L 2000 A direct comparison of wet, dry and insulating bioelectric recording electrodes *Physiol. Meas.* **21** 271–83

[101] Woo E J, Hua P, Webster J, Tompkins W and Pallas-Areny R 1992 Skin impedance measurements using simple and compound electrodes *Med. Biol. Eng. Comput.* **30** 97–102

[102] Kusche R, Kaufmann S and Ryschka M 2019 Dry electrodes for bioimpedance measurements - Design, characterization and comparison *IOP Biomed. Phys. Eng. Express* **5**

[103] Fsis U *How Temperatures Affect Food*

[104] Vescio G, Rosell J, Nescolarde L and Giovinazzo G 2011 Muscle fatigue monitoring using a multifrequency bioimpedance technique *IFMBE Proceedings* vol 37 (Springer, Berlin, Heidelberg) pp 1257–60

[105] Dzwonczyk R, Del Rio C, Brown D A, Michler R E, Wolf R K and Howie M B 2004 Myocardial electrical

impedance responds to ischemia and reperfusion in humans *IEEE Trans. Biomed. Eng.* **51** 2206–9

[106] Bragos R, Riu P J, Warren M, Tresanchez M, Carreno A and Cinca J 1996 Changes in myocardial impedance spectrum during acute ischemia in the in-situ pig heart *Annual International Conference of the IEEE Engineering in Medicine and Biology - Proceedings* vol 5 (IEEE) pp 1953–4

[107] Huff-Lonergan E and Lonergan S M 2005 Mechanisms of water-holding capacity of meat: The role of postmortem biochemical and structural changes *Meat Science* vol 71 (Elsevier) pp 194–204

[108] Bîrlea N M, Bîrlea S I and Toşa V 2009 The skin's electrical asymmetry *J. Phys. Conf. Ser. OPEN ACCESS* **182** 12020

[109] Shin S C, Lee S, Lee T, Lee K, Lee Y S and Kang H G 2018 Two electrode based healthcare device for continuously monitoring ECG and BIA signals *2018 IEEE EMBS International Conference on Biomedical and Health Informatics, BHI 2018* vol 2018-January (Institute of Electrical and Electronics Engineers Inc.) pp 141–4

[110] Geddes L A and Valentinuzzi M E 1973 Temporal changes in electrode impedance while recording the electrocardiogram with "Dry" electrodes *Ann. Biomed. Eng.* **1** 356–67

[111] Yokus M A and Jur J S 2016 Fabric-based wearable dry electrodes for body surface biopotential recording *IEEE Trans. Biomed. Eng.* **63** 423–30

[112] Lu F, Wang C, Zhao R, Du L, Fang Z, Guo X and Zhao Z 2018 Review of stratum corneum impedance measurement in non-invasive penetration application *Biosensors* **8** 31

[113] Kobelev A V., Shchukin S I and Leonhardt S 2019 Application of tetrapolar electrode systems in electrical impedance measurements *Biomed. Eng. (NY).* **52** 383–6

[114] Cömert A and Hyttinen J 2014 Impedance spectroscopy of changes in skin-electrode impedance induced by motion *Biomed. Eng. Online* **13** 149

[115] Oliveira C C, Machado da Silva J, Trindade I G and Martins F 2014 Characterization of the electrode-skin impedance of textile electrodes *Proceedings of the 2014 29th Conference on Design of Circuits and Integrated Systems, DCIS 2014* (Institute of Electrical and Electronics Engineers Inc.)

[116] Ninagawa T 2012 Measurement of microclimate within clothing using the combination technique of infrared ray absorption method and holographic interferometry *Open Appl. Phys. J.* **5** 54–9

[117] Bernengo J C and de Rigal J 2017 Physical methods to measure stratum corneum water content in vivo *Agache's Measuring the Skin: Non-invasive Investigations, Physiology, Normal Constants: Second Edition* (Springer International Publishing) pp 299–340

[118] Shinwari M W, Zhitomirsky D, Deen I A, Selvaganapathy P R, Deen M J and Landheer D 2010 Microfabricated reference electrodes and their biosensing applications *Sensors* **10** 1679–715